Grant Agreement: 825027

Start date: 01.01.2019

Duration: 44 months

AD ASTRA Deliverable D2.4

"Accelerated Stress Test Protocols for Specific SOC components in CHP and P2X Application Areas"

Due date of deliverable: 31.08.2022

Lead Beneficiary: IEES

Nature: Report

Revision	Submission date	Description
1	20.06.2022	Version 1
2	08.09.2022	Version 2
3	27.10.2022	Version 3
4	31.10.2022	Version 4
5	08.11.2022	Final Version

Dissemination level (mark with an x the relevant)		
PU	Public	**x**
CO	Confidential, only for members of the consortium (including the Commission Services)	

Acknowledgements: This project has received funding from the Fuel Cells and Hydrogen 2 Joint Undertaking (now Clean Hydrogen Partnership) under Grant Agreement No 825027. This Joint Undertaking receives support from the European Union's Horizon 2020 Research and Innovation program, Hydrogen Europe and Hydrogen Europe Research.

Report title: "Accelerated Stress Test Protocols for Specific SOC components in CHP and P2X Application Areas"	Deliverable No D2.4
Responsible author: Daria Vladikova	

Authors:

Daria Vladikova, Milena Krapchanska, Blagoy Burdin, Asrar Sheikh, IEES

Davide Pumiglia, Massimiliano Della Pietra, Stephen McPhail, ENEA

Jerome Laurencin, Maxime Hubert, CEA

Roberto Spotorno, Paolo Piccardo, Daniele Paravidino, UNIGE

Anke Hagen, Aiswarya Krishnakumar, DTU

Aline Léon, EIFER

Hamza Moussaoui, Samaneh Daviran, Jan Van herle, EPFL

Dario Moninaro, SolidPower

Christian Geipel, Kai Herbrig, Hassan Javed, Sunfire

Summary

Deliverable 2.4 "Accelerated Stress Test Protocols for Specific SOC Components in CHP and P2X Application Areas" can be regarded as the final product of AD ASTRA project which aimed at defining Accelerated Stress Testing (AST) protocols deduced from a systematic understanding of degradation mechanisms of aged components in Solid Oxide Cells (SOC), operating in both fuel cell and electrolysis modes. Special attention was given to the organization of the work, combining existing information, including data from long term field tests performed by partners before the start of the project, as well as accumulated data from big number of experiments implemented in the frames of the project. A combination of testing and characterization of: (i) new samples designed for AD ASTRA, and (ii) old samples from previous tests were used. The Design of Experiments (DoE) was carried out in an iterative approach, based on three cycles with well defined experimental rounds. The main goal of the DoE was to optimize the number of experiments in respect to the limited resources as time, equipment, personnel etc., gathering maximum of information. During Cycle 1 information derived from previous experience in GENIUS on long term tests on stacks was exploited. For the analysis three factors were chosen. The results showed that at least 11 stacks were needed which was not acceptable for the project resources. That is why the efforts were concentrated on micro samples (button cells) which ensure reliable

information accumulated for shorter time and less resources. The DoE approach supported ease interpretation, comparison and elaboration of data, specifying: (i) *in-situ* aggravating tests; (ii) *ex-situ* component ageing; (iii) test conditions, (iv) stressors, (v) test equipment, (vi) targeted degradation phenomena, (vii) accelerated stress level etc.

A special data bank was introduced as a friendly tool for the organization, monitoring and management of the project resources. It stored in an organized way inputs from field tests, previous projects, as well as the data generated within the project experimental campaigns: data for the samples design, fabrication, test conditions and procedures, stressors, testing, characterization, thus ensuring the ID of every sample "form cradle to grave". The data were schematized, analysed and prepared for the development of the AST protocols.

As a final result 12 AST protocols were elaborated. They were divided in 2 main groups in respect to the approach for introduction of the stressor:

- *In-situ* aggravated tests for accelerated observation and testing of degradation phenomena in relation to test input parameters (marked in the title of the protocol) which generate harsh operational conditions (6 Protocols);
- *Ex-situ* artificial ageing (marked in the title of the protocol) which reproduces faster the degraded condition of critical component or interface in respect to calendar aging in nominal conditions (6 Protocols).

The protocols follow one and the same structure, giving information about: selected AST approach; samples used; experimental set-up; nominal operation parameters; stressor and stress factor; quantification of the degradation at nominal conditions and under stress test; acceleration factor. In the end of the protocol there is an example showing its application and the results obtained.

Key words: Accelerated Stress Tests, Solid Oxide Cells, Artificial Aging, Aggravated conditions, Redox Cycling, *i-V* curves, Impedance Spectroscopy.

TABLE OF CONTENTS

1. INTRODUCTION

1.1. Description of the deliverable content and purpose

Solid Oxide Cells (SOC) have an important role and hold great promise with their diverse and versatile portfolio in the energy sector, ensuring opportunities for integration of renewable energy sources into the overall energy system. However, the spectrum of applications still meets some general barriers, summarized as durability and costs. The initial performance degrades over their lifetime due to the effect of use (electrochemical ageing), of time (calendar ageing), of different permanent and/or accidental stress conditions - thermal, current load, mechanical, poisoning etc. Considering the expected useful commercial maintenance-free lifetime of up to 80 000 hours for stationary applications, a challenging objective is to maintain the initial, or close to initial performance for as long as possible.

The work on life time improvement needs long term electrochemical tests for accumulation of reliable data that may continue several years, which is unaffordable for the fast commercialization. A problem-solving approach is the introduction of Accelerated Stress Tests, applying high levels of stress for a shorter period while the experimental conditions should activate the same degradation mechanisms as in non-accelerated testing, thus preventing the system from eventual irreversible changes which may bring to false results. AST is non-destructive method applied for reducing the test time for degradation qualification. It can be performed on cell component, cell, stack component or stack. AST cannot be a self-standing/independent experiment. It needs a benchmark test sample operated at real life (nominal) conditions and fully characterized which will serve as reference for determination of the degradation caused by the stress test. Since there are no definite criteria for the level of acceleration of a specific degradation phenomenon, the selection of aggravating conditions is a critical moment in the AST.

Stress conditions

The AST is performed under operating conditions which stress the test sample (for instance cell), or one of its components in a univocal way. The exaggeration of one of the testing parameters to achieve this is called a stress factor.

There are two approaches which are applied for performance of accelerated stress tests in AD ASTRA Project:

- *In-situ* aggravated tests of cells/stacks: those tests are designed for accelerated registration of degradation phenomena caused by selected harsh values of an input operation parameter as temperature, load current, pressure, or extreme operation regime as thermal or load cycling. The aggravated operational conditions must stress the sample in a representative way while minimizing time and resource expenditure.

- *Ex-situ* artificial ageing of critical cell/stack single component (fuel or oxygen electrode, interconnect) in appropriate accelerating conditions, which reproduce the aged state reached by calendar aging in real life conditions. The level of aging is determined based on analysis of the corresponding components extracted from cell/stack after long term field tests. The artificially aged components can be integrated in an otherwise new cell/stack and further tested *in-situ* in the new configuration and nominal operating conditions, thus defining the effect of single component degradation on the total performance of the system. Another option is the artificial aging of the critical component in the final test assembly (cell, stack) prior to the further testing of the whole configuration. This approach (when possible) is more-simple and eliminates eventual influence of the final technological assembling on the already aged component.

Quantification of degradation

Degradation is most often represented as degradation rate, determined by long term calendar aging in real life (nominal) operation mode or by accelerated stress testing. It is important to have appropriate industrial benchmark data related at least to cell/stack based on same raw materials and operating conditions.

Several approaches for calculation of the degradation rate can be used: (i) increase of the Area Specific Resistance (ASR); (ii) voltage decrease at constant current density; (iii) current decrease at constant voltage. The changes are taken for 1000 hours.

Techniques and approaches for quantification of the degradation:

- In operando measurements. For quantitative evaluation of the accelerated degradation the following electrochemical measurements are applied periodically during the aging tests in accelerated and nominal (reference) conditions:
    - Electrochemical impedance spectroscopy performed in different working points: at OCV and under load. The measurements are used for determination of the ASR (total, ohmic, polarization). EIS data post-processing via DRT (Distribution of Relaxation Times) for example, could provide deeper insights about the limiting phenomena;
    - Total Harmonic Distortion (THD) analysis is used to quantify the non-linearity of system under a faulty operation;
    - Voltage change with time at constant current;
    - Current change with time at constant voltage;
    - Current-voltage curves from which the above-mentioned parameters can also be calculated.
- Post operation characterization of the cell/stack components microstructure. A comparative analysis with pristine sample and sample aged in reference conditions is performed.

Correlation of the long-term degradation at nominal operation conditions with the degradation at AST conditions

The correlation is performed by combination of post-test measurements and numerical or analytical correlations between the real-life aging data and operating reference conditions (or at least the final performance level), and the AST aging data and performed AST conditions that replicate the calendar aged state. The correlation determines at least the Acceleration Factor (AF) in terms of timing (*t*):

$$\mathrm{AF} = \frac{t_{long\ term\ test}}{t_{AST\ bringing\ to\ the\ same\ degradation}}$$

Taking into consideration that the comparison of aging under real life and accelerated conditions depends on a big number of undefined factors such as raw materials sources and purity, experimental set up (architecture, geometry), size of the samples and technological procedures, lack of sufficient information about the stressors and stress conditions etc., the prepared AST Protocols have qualitative explanations in addition to the quantitative guidelines.

1.2. Deviation from objectives

No deviations are reported from the project objectives for this task and deliverable.

1.3. If relevant: internal property rights

No intellectual property issues are reported.

2. ACCELERATED STRESS TEST PROTOCOLS

This chapter describes the AST Protocols elaborated in AD ASTRA. They are divided in two groups based on the approaches applied for the tests performance: (i) *in-situ* (6 protocols) and (ii) *ex-situ (6 protocols)*.

***In situ* stress test protocols**

2.1. *In-situ* cell reactants (fuel, oxygen and steam) starvation (EPFL)

2.1.1. Description of the AST Approach

The failure modes investigated in this section are fuel starvation and air starvation in fuel cell operation and steam starvation in electrolysis operation. Different combinations of operating parameters are explored to induce these failure modes. This is similar to real operation, in which a critical state or failure mode can also be caused by different scenarios. It also permits a more in-depth analysis of the effect of the different operating parameters combinations.

2.1.2. Experimental samples

The cell used in this work is an ASC made by SOLIDpower, whose fuel electrode and electrolyte are 60 mm in diameter, whereas the oxygen electrode is 40 mm. Therefore, the electrochemically limiting area is that of the oxygen electrode (12,57 cm^2), which must thus be used for normalization.

2.1.3. Experimental set-up

A gold mesh was used as the current collection on the cathode side, and Ni-foam on the anode side, with gold wires for current leads and voltage probes. A K-type thermocouple was positioned next to the cathode. The cell and current collectors were compressed together between spring-loaded flanges using alumina felt insulating layers. The assembly was placed in the middle of a furnace (Rohde). The gas supply was controlled by MFCs (Red-y, Voegtlin).

2.1.4. Nominal operation parameters

Table 1 **Nominal operation parameters.**

Sample type	Operation Mode	Parameter	Units	Value	Remarks
ASC	SOFC/SOE	Temperature	°C	750°C	
		Pressure	mbar	Ambient	
		Fuel	Nml/min/cm^2	SOFC: H_2/N_2 60/40 % 15,91 SOE: H_2O/H_2 90/10 % 15,91	Nominal surface normalized flow rates are relatively high for single cells compared to stacks
		Oxidant	Nml/min/cm^2	Synthetic air: N_2/O_2 79/21 % 23,87	Same remark as above
		Current Density	A/cm^2	No constraint	Nominal power is rather dictated by voltage than current
		Voltage	V	SOFC: OCV down to 0,70V SOE: Thermoneutral voltage 1,29 V up to 1,35 V	Nominal voltage could change with the cell state of health. 0,65 V and 1,4V, in SOFC and SOE modes respectively, if SoH is low
		Fuel Utilization/ Steam Conversion	%	FU_{max}: 80 SC_{max}: no constraint	Up to 82 % FU is acceptable
		Oxidant Utilization	%	Not limiting (Typically around 33 %)	Air is mainly used to control temperature.Oxygen is typically 3-4 times more than needed for the electrochemical reactions

2.1.5. Stressor (stress parameter) and stress factor

Fuel starvation: FU is increased by decreasing H_2 content. FU values varied from nominal to 93 %.
Oxygen starvation: OU is increased by decreasing oxygen content. OU values ranged from nominal to 90 %.
Steam starvation: SC is increased by decreasing steam content. SC values ranged from normal to 76 %.

2.1.6. Presentation and quantification of the degradation at nominal conditions and under stress test

Regular polarization curves, EIS complemented by DRT, and THD were acquired to *in-situ* monitor and quantify the degradation effect and compare it to the reference operation case. The procedure is explained for every AST in the following section.

2.1.7. Description of the AST procedure

Fuel Starvation:

Scenario 1: Fuel starvation at constant voltage

Nine EIS and THD measurements are performed at constant voltage (0,8 V), while the amount of H_2 in N_2 was gradually decreased. Doing so, the current density decreases, but the FU increases. The voltage of 0,8 V is chosen to be close to real operating conditions for which lower voltages are recommended to reach a high FU, but without falling below the critical voltage of around 0,7 V (approximately the equilibrium voltage between NiO and Ni). The compositions range from 100 % down to 8 % H_2 content. For each composition a polarization curve was recorded. The fuel was a dry mixture of H_2 and N_2 only. The constant operating parameters of this experiment were: 750°C cell temperature, radially outward fuel flow, 150 Nml/min fuel flow rate, 300 Nml/min air flow rate and O_2/N_2 = 21/79 air composition.

Scenario 2: Fuel starvation at constant composition

In this experiment, the fuel composition is maintained at H_2/N_2 = 30/70, while the polarization was gradually changed to increase the FU.

Scenario 3: Fuel starvation at constant current

In this experiment, the current density is kept constant (318 mA/cm^2) for EIS/THD measurements, while the fuel composition was gradually changed to increase the FU.

Oxygen Starvation:

Scenario 1: Oxygen starvation by varying synthetic air composition (at constant flow)

The amount of O_2 in the air was gradually lowered, while the total air flow rate was kept constant at 300 Nml/min. Polarization curves were recorded for seven different compositions with an O_2 content ranging from 50 % to 6 %. For each composition EIS and THD measurements were performed at 0,8 V in galvanostatic mode. The OU ranges from 21 % to 89 %.

Scenario 2: Oxygen starvation by varying air flow rate (at constant real air composition 21/79)

In this experiment the total air flow rate is varied from 300 to 100 Nml/min, while the air composition was kept constant at ambient conditions O_2/N_2 = 21/79 to increase the OU. This method is of higher practical relevance, since most SOFCs are operated with ambient air and therefore constant composition. However, in case of a problem with the air supply system, the air flow rate might change, which resembles this experiment. The air flow rates chosen for this experiment are such that the O_2 flow rates are the same as in the compositions of the previous experiment. Polarization curves were recorded for five different air flow rates. Seven EIS and THD measurements were performed in galvanostatic mode, first at 0,8 V and ultimately at lower voltages to further increase the OU (> 80 %).

Steam Starvation:

In this experiment the fuel composition is gradually changed from a high steam content (H_2O/H_2 = 80/20) to a low steam content (H_2O/H_2 = 20/80). In total, *i-V* curves for seven different compositions are recorded. For each composition an EIS and THD measurement was performed at 1,35 V in potentiostatic mode with a constant amplitude of 50 mV = 3,7 %, yielding SC rates between 52 % and 76 %. Moreover, the constant operating parameters during this experiment were: 750°C cell temperature, 150 Nml/min fuel flow rate, 300 Nml/min air flow rate, and O_2/N_2 = 21/79 air composition.

2.1.8. Correlation of the long-term degradation at nominal operation conditions with the degradation at accelerated stress conditions

The possible degradation mechanisms due to reactants starvation are:

- Ni reoxidation at high FU in SOFC mode
- Ni migration due to the high gradients of (humidity, temperature, …) mainly in SOE mode
- Formation of ZrO_2 nano-particles on Ni Surface: During Zr re-oxidation to ZrO_2, due to high overpotential, when the contact between Ni and YSZ is lost, nanoparticles are precipitated around the Ni particles in SOE mode.
- Delamination of the positive electrode due to the build-up of oxygen pressure due to a limited oxygen flux, or due to the $SrZrO_3$ secondary phase formation within the GDC barrier layer, mainly in SOE mode >≈ 1.5 V.
- LSCF and LSC demixing due to the segregation of SrO, which may then diffuse towards interface with electrolyte, or react with foreign compounds, or to the $SrZrO_3$ and $La_2Zr_2O_7$ insulating secondary phase formation within the GDC barrier layer, or to the $SrCrO_4$ formation into and onto LSCF and LSC, mainly in SOE mode.
- YSZ electrolyte ionic conductivity loss and electric conductivity gain due to its reduction in SOE mode >≈ 1.8 V, in the absence of steam, causing higher ohmic resistance and short-circuit.

In real-life application, reactant starvation arises during operation because of several issues. One of the most common scenarios is a leakage in the stack that will deprive some cells or parts of cells of the fuel, steam or air. A gas shortage may also obviously trigger this fault. It not properly detected and identified, reactant starvation will accelerate the overall degradation and eventually cause a premature stack end-of-life. The accelerated factor of the proposed tests can reach values as high as 10 compared to nominal operation.

2.2. *In-situ* cell 'overpotential' aging (EPFL)

2.2.1. Description of the AST Approach

High overpotential tests are performed by operating the cell beyond the recommended voltage range (c.f. Section 2.1.4.) in potentiostatic setting. The process should be induced progressively and iteratively to acquire a clear picture of the cell answer.

In SOFC mode, the cell is driven from the nominal voltage range of OCV - 0,7 V down to values as low as 0,5 V while keeping the other parameters unchanged. This will have the effect of increasing the temperature, current, and thus the fuel utilization eventually causing some local Ni reoxidation and material degradation.

In SOE mode, the cell is similarly driven from the nominal voltage range of 1,29 - 1,35 V up to 1,6 V while keeping the other parameters unchanged. Voltages as high as 1,8 V or even 2 V to investigate very extreme conditions. This will have the effect of increasing the steam conversion and inducing some steam starvation. YSZ reduction and Ni migration are expected in this case among other degradation phenomena.

Sensitivity analyses to operating temperature, gases flowrates, and to EIS and THD parameters bring deeper insights and a more complete picture of the underlying degradation phenomena.

2.2.2. Experimental samples

The cell used in this protocol is an ASC made by SOLIDpower, whose fuel electrode and electrolyte are 60 mm in diameter, whereas the oxygen electrode is 40 mm. Therefore, the electrochemically limiting area is that of the oxygen electrode (12,57 cm^2), which must thus be used for normalization.

2.2.3. Experimental set-up

A gold mesh was used as the current collection on the cathode side, and Ni-foam on the anode side, with gold wires for current leads and voltage probes. A K-type thermocouple was positioned next to the cathode. The cell and current collectors were compressed together between spring-loaded flanges using alumina felt insulating layers. The assembly was placed in the middle of a furnace (Rohde). The gas supply was controlled by MFCs (Red-y, Voegtlin).

2.2.4. Nominal operation parameters

Table 2 **Nominal operation parameters.**

Sample type	Operation Mode	Parameter	Units	Value	Remarks
ASC	SOFC/SOE	Temperature	°C	750°C	
		Pressure	mbar	Ambient	
		Fuel	Nml/min/cm^2	SOFC: H_2/N_2 60/40 % 15,91 SOE: H_2O/H_2 90/10 % 15,91	Nominal surface normalized flow rates are relatively high for single cells compared to stacks
		Oxidant	Nml/min/cm^2	Synthetic air: N_2/O_2 79/21 % 23,87	Same remark as above
		Current Density	A/cm^2	No constraint	Nominal power is rather dictated by voltage than current
		Voltage	V	SOFC: OCV down to 0,70 V SOE: Thermoneutral voltage 1,29 V up to 1,35 V	Nominal voltage could change with the cell state of health. 0,65V and 1,4V, in SOFC and SOE modes respectively, if SoH is low.
		Fuel Utilization/ Steam Conversion	%	FU_{max}: 80 SC_{max}: no constraint	Up to 82 % FU is acceptable
		Oxidant Utilization	%	Not limiting (Typically around 33 %)	Air is mainly used to control temperature. Oxygen is typically 3-4 times more than needed for the electrochemical reactions.

2.2.5. Stressor (stress parameter) and stress factor

The stress parameter here is the cell's voltage as described in Section 2.2.1.

2.2.6. Presentation and quantification of the degradation at nominal conditions and under stress test

Regular polarization curves, EIS complemented by DRT, and THD were acquired to *in-situ* monitor and quantify the degradation effect and compare it to the reference operation case.

2.2.7. Description of the AST procedure

In this experiment the voltage is gradually decreased in SOFC mode, or increased in SOE mode out of the nominal range while maintaining the other parameters unchanged. Hold times should be long enough to reach the steady state operation. Recovery periods of times can also be included to investigate the reversibility of the damage, and the time needed.

2.2.8. Correlation of the long-term degradation at nominal operation conditions with the degradation at accelerated stress conditions

The polarization overpotentials are unavoidable and could only be kept within a safe range. The limits of healthy operation are not universally established because they may depend on many parameters like the cell's SoH, but it is commonly agreed to keep the cell voltage above 0.7 V in fuel cell mode and below 1.4 V in electrolysis operation. This can be fulfilled by keeping the operating parameters (temperature, current, reactants mass flows, …) in the nominal range. However, in a 60-80 cells full stack, the operating conditions may widely change from the top to the bottom cell, and also within the same cell. For example, the current could be more than 50% higher at inlet compared to the cell mean value. The temperature at the cell's outlet region or the last cell could be as higher as 100 ^{o}C compared to the coldest spot. Therefore, these local heterogeneities between cells can be problematic during stack operation as only the mean voltage over the cells is measured which could overshadow a large disparity between the individual cell voltages. Finally, even at a same global voltage, on a local scale a single cell shows different contributions to the total overpotential from inlet to outlet. Indeed, the inlet region is mostly dominated by the activation losses due to the high reactants/products ratio, while the outlet region is dominated by concentration losses due to reactants starvation.

The possible degradation mechanisms due to high overpotential are the same as the ones explained in the previous section of reactant starvation.

The proposed AST protocol aims at reaching very high overpotentials in a progressive way in order to investigate at which threshold we induce irreversible damage. The acceleration factor can then reach very high values (as high as few hundreds) for the highest overpotential values.

2.3. *In-situ* cell 'T-cycle' aging (EPFL)

2.3.1. Description of the AST Approach

Thermal Expansion Coefficient (TEC) mismatch can be a possible reason for cathode delamination. Fast thermal cycling test is designed to study the thermal stress role in cathode delamination mechanism or any other failures.

2.3.2. Experimental samples

Solidpower pristine cells were tested.

2.3.3. Experimental set-up

Such fast-thermal cycling requires an advanced furnace which was built in our group (GEM) that allows significantly rapid thermal cycling both in heating and cooling and therefore both a faster turn-over in testing time as well as more harsh test conditions (fast ramps). Cooling system was designed to achieve homogeneous cooling.

2.3.4. Nominal operation parameters

The test protocol is considered as: 600-1000°C/hour heating/cooling rate with upper and lower temperatures of 250°C and 850°C, respectively. The dwell time period at lower and upper temperatures is 10 min and is kept as short as possible to impose a rapid thermal cycling.

Table 3 **Operating parameters of thermal cycling**

Sample type	Parameter	Units	Value
Pristine cell (SP)	Temperature (upper)	°C	850
	Temperature (lower)	°C	250
	Heating cooling ramp	°C/hour	600 - 1000
	No. of cycles	-	50 - 100 - 150 - 200 - 250
	Dwell time	min	≤ 10
	Pressure		atmospheric

2.3.5. Stressor (stress parameter) and stress factor

- Heating/cooling rate: the baseline for heating/coming ramp was 600°C/hours which was increased to 850°C/hours and 1000°C/hours,
- Number of cycling: 50 cycles is considered the baseline and in the stressed condition it was increased to 100, 150, 200, and 250 cycles.

2.3.6. Presentation of the degradation at nominal conditions and under stress test

SEM image analysis is used to check if any delamination, crack or failure happened during the test (an example is presented in annex).

2.3.7. Quantification (measurement) of the degradation

In the present test, the quantification of the degradation relies of SEM image processing. In case any delamination was observed.

2.3.8. Description of the procedure

Cycling test was performed on five pristine cells run for 50, 100, 150, 200, and 250 cycles.

2.3.9. Correlation of the long-term degradation at nominal operation conditions with the degradation at accelerated stress conditions

Microstructure analysis on SEM cross section images of T-cycled tested cells determine if TEC mismatch is the reason for oxygen electrode delamination in long-term test or if the electrochemical effect is dominant.

2.3.10. Annex (with illustrations) for demonstration of the AST Protocol performance

Pristine cells were tested under thermal cycling based on the AST protocol summarized in Table 3. One of the tested samples cycled over 250 times (the maximum cycling number and as the harsher condition) is presented here as an example. The sample was started heating up with the ramp of

800ºC/hour, kept constant at 850ºC for 10 min, then heat exchanger for cooling system starts cooling down (to 250ºC) the sample to help reaching the same ramp for the heat up. Cycling trend is displayed in Figure 1.

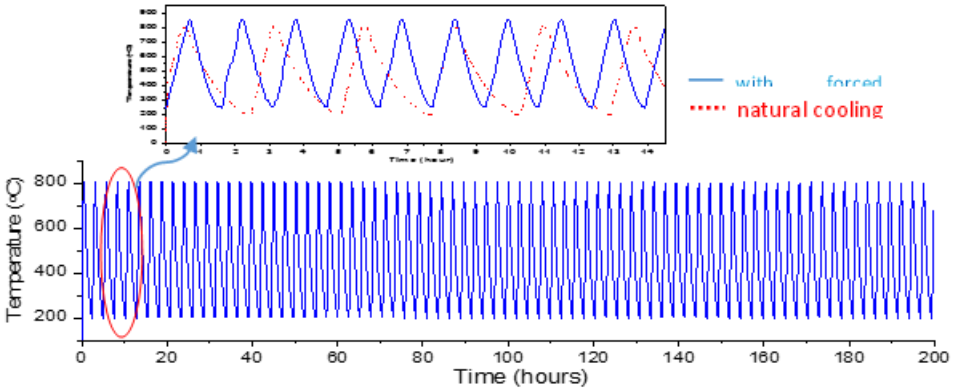

Figure 1 **Fast thermal cycling of pristine cell.**

SEM cross-section and image analysis for the sample cycled 250 times is shown in Figure 2. The interface between the electrode and CGO barrier layer displayed no delamination or failure from thermal cycling test up to 250 times. Thus, it means that thermal shock and TEC mismatch probably is not the reason for oxygen electrode delamination but electrochemical effects is probably the reason.

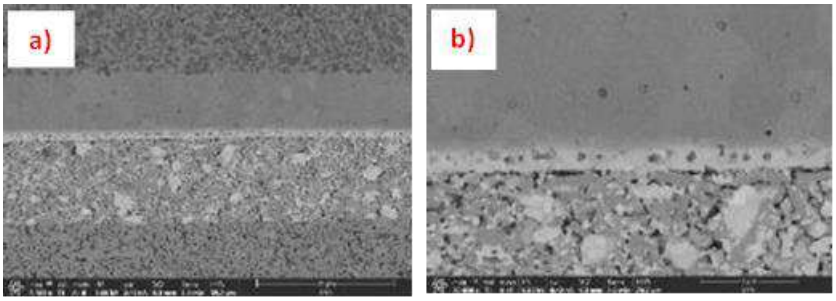

Figure 2 **Cross-section microstructure of pristine cell cycled over 250 times.**

2.4. *In-situ* cell aging with high temperature, steam for the air electrode (CEA)

2.4.1. Description of the AST Approach

The impact of temperature and humidity in the air at the O_2 electrode are used as stress factors to accelerate the degradation of the O_2 electrode in H_2 electrode supported cell tested in electrolysis mode. In both cases, the Sr segregation (and hence the decomposition of the air electrode in LSCF) is expected to be aggravated with respect to the normal condition (dry air or temperature lower than 800°C). The AST protocols are thus controlled by two main parameters, the humidity at the air side and the cell temperature.

2.4.2. Experimental samples

The protocols have to be applied on button cells (ACS). For the effect of temperature, the ID of the samples are 0048_CEA_New and 0047_CEA_New (for ageing at 850°C and 750°C at - 0,75 A/cm², respectively). For the effect of humidity at the air side: 0050_CEA_New and 0049_CEA_New (for ageing at 8 % of steam in the air flow and dry condition at 750°C - 0,75 A/cm², respectively).

2.4.3. Experimental set-up

A test rig for the cells electrochemical characterization of in electrolysis mode is required up to a temperature of 850°C. The tightness of hydrogen compartment is needed with a glass sealing able to withstand high temperature (T≤850°C) (cf. annex for the details). The air flow at the O_2 electrode needs to be humidified up to 8 % using a classical bubbler.

2.4.4. Nominal operation parameters

Table 4 **Nominal operation parameters.**

Sample type	Operation Mode	Parameter	Units	Value	Remarks
Anode supported	Electrolysis	Temperature	°C	750	
		Pressure	atm	1	
		Fuel	Nml/min/cm^2	12	Single gas or gas mixture
		Water	% in respect to the fuel	90	
		Air	Nml/min/cm^2	36	Synthetic gas
		Current Density	A/cm^2	- 0,75	
		Steam conversion	%	50	
		Oxidant Utilization	%	Non applicable	
		Other depending on the protocol		Non applicable	

2.4.5. Stressor (stress parameter) and stress factor

Stress factor on temperature: temperature has been increased from 750°C (0047_CEA_New) to 850°C (0048_CEA_New).

Stress factor on humidity: Dry air at the O_2 electrode (0049_CEA_New) has been replaced by humidified air at 8 % (0050_CEA_New).

2.4.6. Presentation and quantification of the degradation at nominal conditions and under stress test

Table 5 **Results on the batch tested for the impact of humidity**

Degradation rate	Nominal condition	Stress factor: Humidity at the air electrode
$\mathrm{DR}/\% = \frac{\left(U_{cell}^{aged} - U_{cell}^{t=0}\right)}{U_{cell}^{t=0}} 100 \cdot \frac{1000}{t_{aging}}$ *(1)*	2,4 %.kh^{-1}	3,9 %.kh^{-1}

$DR/\% = \frac{\left(ASR_{cell}^{aged} - ASR_{cell}^{t=0}\right)}{ASR_{cell}^{t=0}} 100 \cdot \frac{1000}{t_{aging}}$ *(2)*	15,5 %.kh^{-1}	21,8 %.kh^{-1}

(1) Cell voltage measured at - 0,75 A/cm^2 at t = 0 and t = 2000 hrs (T = 750°C).

(2) ASR measured by EIS at i_{dc} = - 0,75 A/cm^2 at t = 0 and t = 2000 hrs (T = 750°C).

Table 6 **Results on the batch tested for temperature**

Degradation rate	Nominal condition	Stress factor: temperature
$DR/\% = \frac{\left(U_{cell}^{aged} - U_{cell}^{t=0}\right)}{U_{cell}^{t=0}} 100 \cdot \frac{1000}{t_{aging}}$ *(1)*	1,8 %.kh^{-1}	1,4 %.kh^{-1}
$DR/\% = \frac{\left(ASR_{cell}^{aged} - ASR_{cell}^{t=0}\right)}{ASR_{cell}^{t=0}} 100 \cdot \frac{1000}{t_{aging}}$ *(2)*	17 %.kh^{-1}	14 %.kh^{-1}
$DR/\% = \frac{\left(R_{Ohm}^{aged} - R_{Ohm}^{t=0}\right)}{R_{Ohm}^{t=0}} 100 \cdot \frac{1000}{t_{aging}}$ *(3)*	9 %.kh^{-1}	17 %.kh^{-1}

(1) Cell voltage measured at - 0,75 A/cm^2 at t = 0 and t = 2000 hrs (measured in the same condition before the ageing test at 850°C).

(2) ASR measured by EIS at i_{dc}= - 0,75 A/cm^2 at t = 0 and t = 2000 hrs (measured in the same condition before the ageing test at 850°C).

(3) Ohmic resistance measured by EIS at i_{dc}= - 0,75 A/cm^2 at t = 0 and t = 2000 hrs (measured in the same condition before the ageing test at 850°C).

2.4.7. Description of the AST procedure

Before durability tests – The cell is heated up to 800°C at a rate of 1°C/min. The reduction of the Ni-based cermet is performed at 800°C by gradually increasing the amount of hydrogen while the amount of nitrogen was decreased. The total flow rate is maintained at the constant value of 4 NmL/min/cm^2. Each step lasted from 5 to 30 minutes until the OCV stabilization. After 12 hours, the gas flows is modified to reach a total flow rate of 12 NmL/min/cm^2, with a composition of 90 vol. % H_2O and 10 vol. % H_2 on the H_2 electrode side. On the O_2 electrode side, the sweeping gas flow rate (synthetic air, with or without addition of humidity at 8 %) is fixed to 36 NmL/min/cm^2.

AST Procedure for the durability using humidity or temperature as stress factor for the O_2 electrode – The durability tests are performed in a galvanostatic mode. A current density of - 0,75 A/cm^2 is applied to the cell at the operating conditions previously reported (temperature and gas composition) which corresponds to a steam conversion of 50 %. A first durability test is performed the nominal condition by supplying dry synthetic air at the O_2 electrode with an inlet flow rate of 36 NmL/min/cm^2. At the cathode side, the total flow rate was 12 NmL/min/cm^2 (90 vol. % H_2O and 10

vol. % H_2). The second test is performed in the same operating conditions by adding 8 vol. % of moisture at the air flow or by increasing the temperature at 850°C. The cells are tested for 2000 hours at least.

2.4.8. Correlation of the long-term degradation at nominal operation conditions with the degradation at accelerated stress conditions

Stress factor on humidity for the oxygen electrode: the correlation can be simply related to the acceleration factor (AF) in terms of timing (t) for the degradation on the cell voltage

$$\mathrm{AF} = \frac{t_{long\ term\ test}}{t_{AST\ bringing\ to\ the\ same\ degradation}} = 4$$

Stress factor on temperature for the oxygen electrode: the high temperature accelerates the formation of zirconates at the electrolyte (cf. annex) and can also affect the inter-diffusion layer in the electrolyte. For this reason, the acceleration factor should be defined in terms of Ohmic resistance.

2.4.9. Annex *(with illustrations)* for demonstration of the AST Protocol performance

2.4.9.1. Impact of temperature on the O_2 electrode degradation

The results on the impact of temperature on the O_2 electrode are thoroughly presented in F. Monaco, D. Ferreira-Sanchez, M. Hubert, B. Morel, D. Montinaro, D. Grolimund, J. Laurencin, Oxygen Electrode Degradation in Solid Oxide Cells Operating in Electrolysis and Fuel Cell Modes: LSCF Destabilization and Inter-Diffusion at the Electrode/Electrolyte Interface, *Inter. J. of Hydrogen Energy*, 46 (62) (2021) 31533-31549 (article available in the repository: https://hal.archives-ouvertes.fr/hal-03543584).

Some of the main characteristic of the experimental setup and results are summarized hereafter:

a) Samples: Typical hydrogen supported cells have been used for this study. They are composed of a dense electrolyte made of 8 YSZ having a thickness of ≈ 8 µm sandwiched between the two electrodes. The hydrogen electrode consists in a thick Ni-YSZ porous cermet (≈ 260 µm) whereas the oxygen electrode has a multilayer structure with a total thickness of ≈ 60 µm. This assembly is composed of a LSCF-GDC ($La_{0.6}Sr_{0.4}Co_{0.2}Fe_{0.8}O_{3-\delta}$ - $Gd_{0.2}Ce_{0.8}O_{2-\delta}$) composite (≈ 16 µm) associated to a LSCF layer (≈ 20 µm) topped with a current collector made of lanthanum strontium cobaltite ($La_{0.5}Sr_{0.5}CoO_3$, LSC). Finally, a barrier layer of GDC of ≈ 4 µm is added between the oxygen electrode and the electrolyte.

b) Test rig: The experiments in electrolysis mode have been performed in an in-house setup depicted in Figure 3. The test bench is equipped with a Crofer22APU oxygen diffuser, positioned on top of the oxygen electrode, which serves also as current collector. To ensure a good electrical contact and a homogeneous flow path, a gold grid of 100 meshes/cm^2 with a diameter of 34 mm was inserted

between the diffuser and the oxygen electrode surface. A gold wire welded on the pipe close to the grid was used to measure the cell voltage whereas the current was applied directly on the metallic inlet pipe (cf. Figure 3). The cell holder at the hydrogen side was also made of Crofer22APU and a Ni grid of 100 meshes/cm^2 has been chosen as current collector in contact with the hydrogen electrode. As for the oxygen electrode, a gold wire welded directly to the Crofer22APU support close to the Ni grid, has been used to measure the cell voltage whereas the current was applied from the metallic pipe (Figure 3). To ensure the gas tightness and the electrical insulation between the two electrodes, a ceramic glass seal is deposited at the periphery of the electrolyte. Finally, a loading of 0,4 kg/cm^2 has been applied on the cell to minimize the contact resistances.

At the inlet of the hydrogen electrode, steam was produced using a steam generator kept in saturated vapor conditions. The steam flow was regulated downstream thanks to a modified Mass Flow Controller (MFC), allowing its operating temperature to be higher than 100°C. A second mass flow controller was used for the hydrogen, and the two fluxes were mixed in the inlet pipe before entering the cell housing. Finally, the outlet gas was sent to a heat exchanger to separate the water from the dry gas.

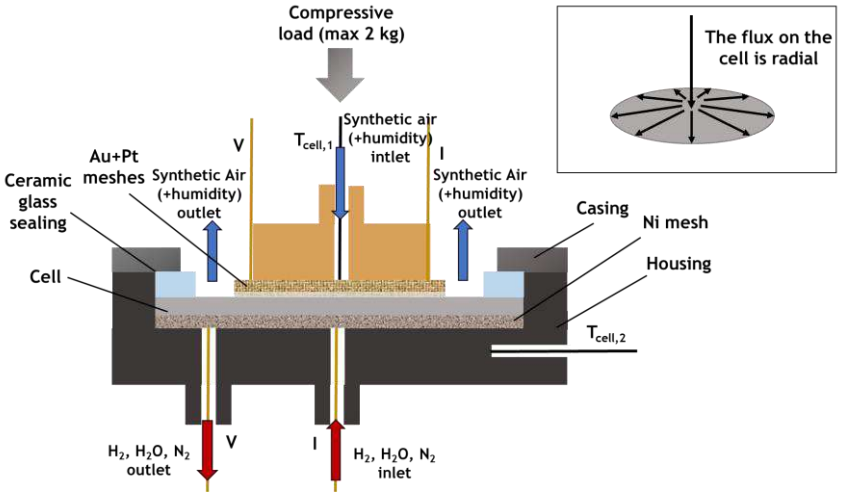

Figure 3 **Schematic representation of the set-up used for the AST protocols.**

c) Test conditions: For cells 0048_CEA_New and 0047_CEA_New, after the reduction of the nickel oxide in the cermet, the polarization curves (*i-V* curves) at 800°C were measured in fuel cell mode sending 100 % H_2 at the hydrogen electrode (flowrate = 6 Nml/min/cm^2). Synthetic air was sent to the oxygen electrode and its flowrate was chosen to have an equivalent air utilization factor of 20 % at $|i_{DC}|$ = 0,75 A/cm^2 for the entire duration of the experiment. After this preliminary characterization, the temperature was increased to 850°C and the gas composition in the hydrogen side was changed to H_2O/H_2 = 90/10 vol. % while raising the total flowrate to 12 Nml/min/cm^2. Once the OCV was stabilized, the *i-V* curves in electrolysis mode was measured. Subsequently, the two durability experiments were conducted. For 0048_CEA_New, the temperature was kept at 850°C and the current was set to - 0,75 A/cm^2. For 0047_CEA_New, instead, the temperature was lowered to 750°C keeping the cell at OCV. After the stabilization of the temperature and the voltage, the

same current as for 0048_CEA_New was applied. During the ageing, the two cells have been operated in galvanostatic mode for ≈ 1800 hours and the evolution of the voltage in each experiment has been recorded every 15 minutes.

d) Main results: The experimental results obtained for 004_CEA_New and 0047_CEA_New are reported in Figure 4. To ensure the same starting point between the two durability experiments, it has been checked that the two cells present the same initial performances. The IV curves obtained in SOFC at 800°C after the reduction of the NiO in the cermet are compared in Figure 4a. The two *i-V* curves are well superposed indicating that the cells exhibit almost identical performances. Moreover, the OCV values obtained in the two cases (1,16 V and 1,15 V for 0048_CEA_New and 0047_CEA_New, respectively) are comparable to the theoretical one (which corresponds to 1,2 V at 800°C if considering 99,6 % of H_2 in the hydrogen side) indicating that there is no significant gas leakage between one electrode and the other.

After this preliminary characterization, the temperature was increased to 850°C and the performances in electrolysis mode have been measured for both cells with a gas composition of H_2O/H_2 = 90/10 vol. % (Figure 4b). In these conditions, the OCV values are almost identical (0,807 V for 0048_CEA_New and 0,805 V for 0047_CEA_New). In addition, the two cells exhibit a similar behaviour in terms of *i-V* curves being perfectly superposed up to i_{DC} = - 0,5 A/cm^2 whereas only a minor difference is found at higher current density (for $|i_{DC}|$ > 0,5 A/cm^2). After the assessment of the initial performances, the durability experiments were conducted and the recorded degradation curves are reported in Figure 4c, in which the evolutions of the cell voltage (at i_{DC} = - 0,75 A/cm^2) are plotted as a function of the ageing time.

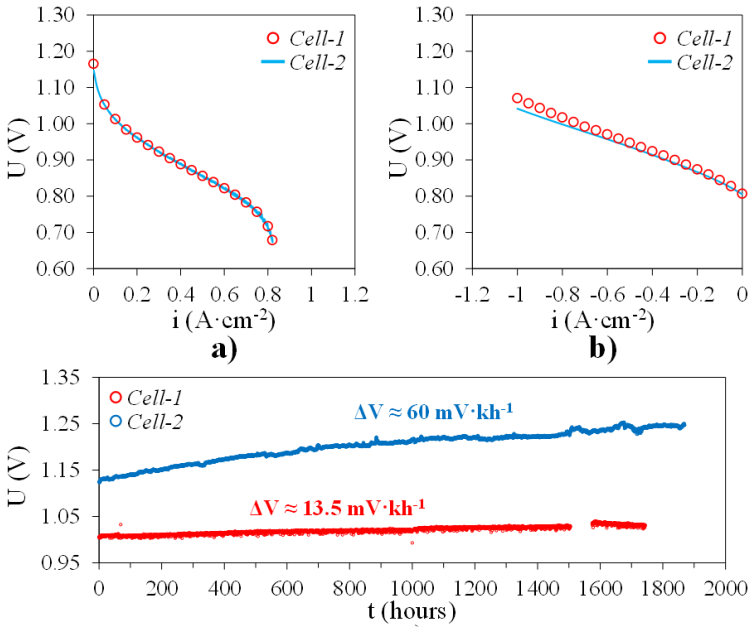

Figure 4 **Experimental results for 0048_CEA_New *(Cell-1)* and 0047_CEA_New (*Cell-2*): a) Initial performances of the cells in SOFC mode at 800°C; b) Initial performances of the cells in SOEC mode at 850°C; c) Durability curves at 850°C (*Cell-1*) and 750°C (*Cell-2*).**

To assess the degradation rates, the impedance diagrams under current at i_{dc}= - 0,75 A/cm^2 have been measured at the same temperature of 850°C at the end of each test and then compared with the initial ones: the results are presented in the table of section 2.4.6. A significant increase in the ohmic resistance has been detected, which is higher for the cell aged at 850°C (0048_CEA_New, ΔR_Ω = 15 mΩ/cm^2/kh or 17 %.kh^{-1}) than for the one aged at 750°C (0047_CEA_New, ΔR_Ω = 8,5 mΩ/cm^2/kh or 9 %.kh^{-1}). This augmentation of the ohmic resistance may originate from different phenomena. It could be mainly ascribed to either a full Ni depletion at the fuel electrode or an accelerated degradation for the O_2 electrode.

e) Post-test characterizations: In our specific case, the SEM observations for the fuel electrode have not revealed any substantial Ni depletion for the two tests that could explain the degradation. However, the thorough characterization of the air electrode by SEM complemented by synchrotron X-ray diffraction and fluorescence have clearly shown a higher LSCF decomposition for the cell aged at 850°C (0048_CEA_New) compared to the one aged at 750°C (0048_CEA_New). For instance, the impact of high temperature (850°C) on the O_2 electrode with the Sr segregation and formation of zirconates at the electrolyte interface is illustrated in Figure 5.

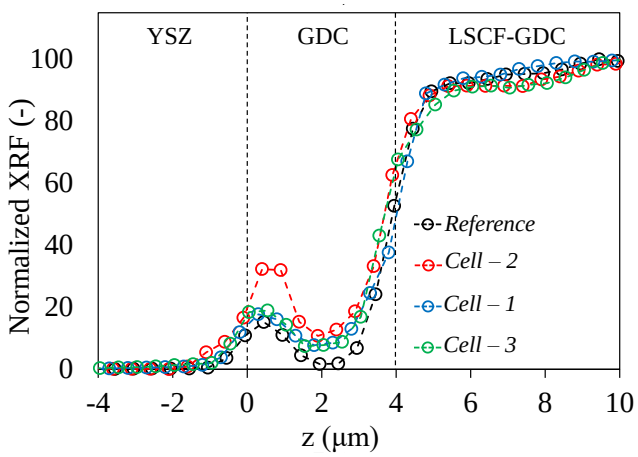

Figure 5 **Comparison of the integrated X-ray fluorescence signal of Sr between the cells aged in the nominal condition at 750°C (*Cell-1* and *Cell-3*: 0047_CEA_New and 0049_CEA_New) and for AST at 850°C (*Cell-2*: 0048_CEA_New).**

2.4.9.2. Impact of humidity on the O_2 electrode degradation

The results on the impact of humidity on the O_2 electrode are thoroughly presented in E. Effori, Modelling of the oxygen electrode for Solid Oxide Cells: study of the reaction mechanism and impact of the degradation PhD thesis, Univ. Grenoble-Alpes, 2021 (PhD thesis available in the repository: https://tel.archives-ouvertes.fr/tel-03377109).

Some of the main characteristic of the experimental setup and results are summarized hereafter:

a) Samples and test rig: the tested cells and the experimental setup are the same than the one used for studying the impact of temperature (cf. section 2.4.9.1).

b) Test conditions: After the cermet reduction, the temperature was decreased down to 750°C with a rate of 1°C/min which is the temperature chosen for the long-term tests. At this reference temperature, polarization curves and EIS diagrams have been recorded. The durability tests were performed in a galvanostatic mode. A current density of - 0,75 A/cm^2 has been applied to the cell at the operating conditions previously reported (temperature and gas composition) which corresponds to a steam conversion of 48 %. A first durability test has been performed by supplying dry synthetic air at the anode side with an inlet flow rate of 36 NmL/min/cm^2. At the cathode side, the total flow rate was 12 NmL/min/cm^2 (90 vol. % H_2O and 10 vol. % H_2). The corresponding cell is thus referenced as 0049_CEA_New. A second test was performed in the same operating conditions by adding 8 vol. % of moisture at the air flow (referenced as 0050_CEA_New). The cells were tested for 2000 h. After 2000 h of operation, final *i-V* curves and EIS diagrams have been recorded at 750°C in the same conditions of the initial characterizations.

c) Main results: As already shown for the impact of temperature (cf. section 2.4.9.1), it has been found that the initial performances of the two tested cells are very similar. In addition, the cell 0050_CEA_New was characterized with *i-V* curves at different steam percentages (0 vol. % - 3 vol. % - 8 vol. %, respectively) in the air flow. As could be expected, the cell performances measured in this moisture range are very close (Figure 6).

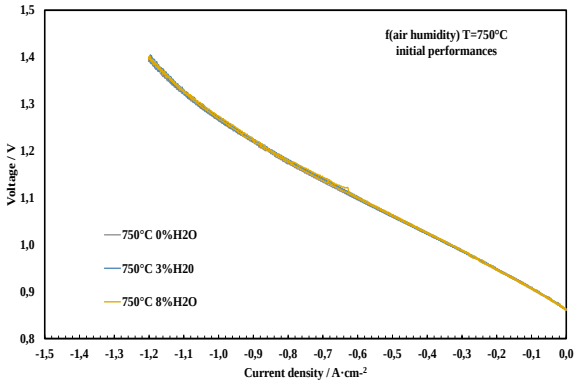

***Figure 6* Initial *i-V* curves as a function of water content in the air flow at the anode side for *Cell-2*. H_2O + H_2 (12 NmL/min/cm^2) at the cathode side, dry synthetic air (36 NmL/min/cm^2) at the anode side.**

The evolution of cell voltage as a function of time during long-term SOEC tests for the two cells are shown in Figure 7. Regardless of the steam content, a steadily increase of the cell voltage has been evidenced in the chosen experimental conditions. The total variation of cell voltage (after 2000 h) has been found to be higher for 0050_CEA_New (ΔV = 45 mV/kh) with respect to 0049_CEA_New (ΔV = 27 mV/kh). The total degradation rate was thus equal to 2,4 %.kh^{-1} and 3,9 %.kh^{-1} at 750°C, respectively (cf. table section 2.4.6). This result indicates that the introduction of steam at the air side accelerates the degradation rate of the tested hydrogen electrode supported cell.

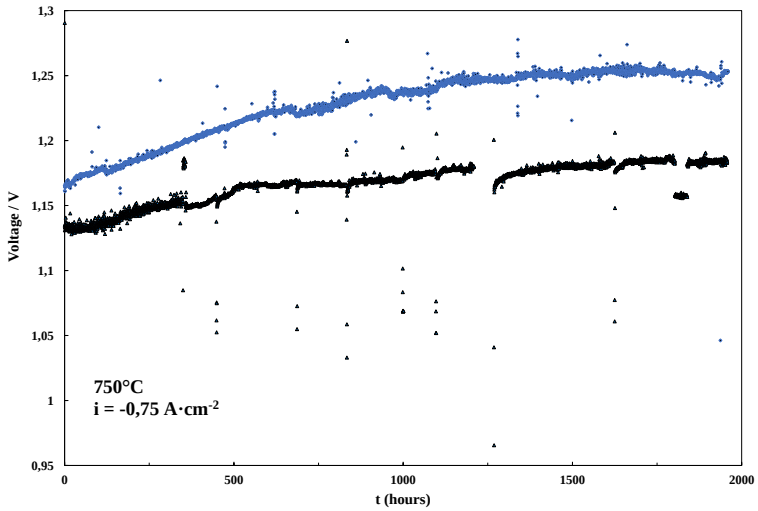

Figure 7 **Time evolution of cell voltages in long-term SOEC tests for 0049_CEA_New (black squares) and 0050_CEA_New (bleu squares) at 750°C, H_2/H_2O 90/10 vol. i = - 0,75 A/cm^2 with a steam conversion of 40 %. H_2O + H_2 (12 NmL/min/cm^2) at the cathode side, dry synthetic air or humid (8 vol. %) air (36 NmL/min/cm^2) at the anode side.**

It is worth noting that after 600 h of operation, the time dependence of the cell voltage slowed down for both cells (Figure 7). Accordingly, two different degradation rates can be considered: a steeper for the first 600 h and a smoother for the remaining 1400 h. Thus, the degradation rates of the cell voltage have also been expressed as voltage losses over time from 600 h to 2000 h. Even after an initial period of 500 h, the degradation rate of the cell voltage is higher under humid air at the anode side (0,6 %.kh^{-1} for 0049_CEA_New and 1,0 %.kh^{-1} for 0050_CEA_New).

Finally, the EIS measurements have shown than the degradation of the series and polarization resistances, and thus of the total cell resistance, are enhanced in humid air (cf. Table 7 and section 2.4.6). Therefore, it can be stated that steam has acted as an accelerating factor for the oxygen electrode degradation. In particular, higher degradation rates of the series and polarization resistances have been measured for this cell. The higher increase of the polarization resistance could be related to the loss of ionic conductivity in the LSCF bulk derived by the higher loss of strontium together with the effect of the surface passivation.

Table 7 **Degradation rates deduced from the impedance spectra measured at i_{dc}= - 0,75 A/cm^2 and 750°C before and after the durability test (degradation rates for the total, ohmic and polarization resistances).**

Degradation rates	Total resistance (% Rt/kh)	Ohmic resistance (% Rs/kh)	Polarization resistance (% Rp/kh)

Dry synthetic air (0049_CEA_New)	15,5	4,7	20,5
Synthetic air humidified at 8 % (0050_CEA_New)	21,8	8,5	35,1

2.5. In-situ cell 'high steam' fuel electrode aging (DTU)

2.5.1. Description of the AST Approach

The impact of high steam in the fuel feed was used as potential stressor for degradation in case of two configurations. ASC and ESC under nominal load conditions. The acceleration studies were performed for fuel cell as well as electrolysis operations. It is expected to accelerate the Ni coarsening and migration effects as compared to low steam conditions under the same nominal load.

2.5.2. Experimental samples

The samples aged under the in-situ aging conditions were single cells with an active area of 4x4 cm^2 received from SolidPower (ASC) and Sunfire (ESC).

ASC samples:

0033_SOL_NEW_002,

0033_SOL_New_003,

0033_SOL_New_004,

0033_SOL_New_005.

ESC samples:

0001_SUN_NEW_006,

0001_SUN_NEW_007,

0001_SUN_NEW_008,

0035_SUN_New_005,

0035_SUN_New_004,

0035_SUN_New_006.

2.5.3. Experimental set-up

Two types of tests were carried out:

- Reference tests,
- Long term tests.

All cells were reduced under safety gas for two hours followed by one hour under pure hydrogen at temperatures defined by the cell manufacturers. The cells were mounted in alumina cell houses with gold seals. Nickel mesh was used as current collectors on the anode side and on the cathode side gold mesh was used. Thermocouples are inserted at the inlet and outlet of the cell in addition to in the furnace. Steam generation occurs within the cell house by combusting hydrogen and oxygen. The flow configuration in the test rigs is co-flow. I-V curves and electrochemical impedance measurements are recorded before, during and after the durability test conditions (Figure 8).

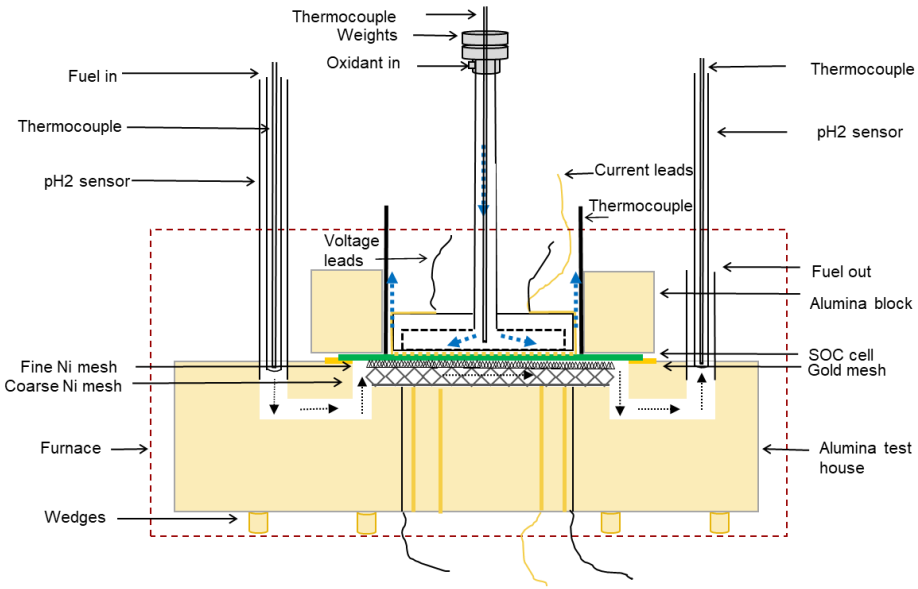

Figure 8 **Ex-situ aging in dual atmosphere setup (full cells).**

2.5.4. Nominal operation parameters

Table 8 and Table 9 contain the operation parameters chosen for the nominal operation.

Table 8 **Nominal operation parameters for ASC configuration.**

Sample type	Operation Mode	Parameter	Units	Value	Remarks
ASC Full cell		Temperature	°C	750	4x4 cm^2 active area
		Pressure		1	
		Fuel	Nml/min/cm^2	0,02 H_2 0,0008 H_2O	Single gas or gas mixture
		Water	% in respect to the fuel	4	
		Oxidant	Nml/min/cm^2	0,06 AIR	Single gas or gas mixture
		Current Density	A/cm^2	0,4	

		Fuel Utilization	%	14	
		Oxidant Utilization	%		
		Other depending on the protocol	%	4	Partial pressure of steam

Table 9 **Nominal Operation parameters for ESC configuration.**

Sample type	Operation Mode	Parameter	Units	Value	Remarks
ESC Full cell		Temperature	°C	850	4x4 cm^2 active area
		Pressure		1	
		Fuel	Nml/min/cm^2	0,01 H_2 0,0004 H_2O	Single gas or gas mixture
		Water	% in respect to the fuel	4	
		Oxidant	Nml/min/cm^2	0,06 AIR	Single gas or gas mixture
		Current Density	A/cm^2	0,2	
		Fuel Utilization	%	14	
		Oxidant Utilization	%		
		Other depending on the protocol	%	2,7	Partial pressure of steam

2.5.5. Stressor (stress parameter) and stress factor

The stressor used in this study was the steam content on the fuel electrode under different operation modes on both the ASC as well as the ESC configurations. The chosen parameters are summarised in the Table 10.

Table 10 **Stressor-steam composition used in case of single cell tests on the two cell configurations.**

Parameters	ASC			ESC	
	96/4	60/40	10/90	96/4	60/40
H_2 flow [l/h]	20	20	13	10	10
H_2O flow [l/h]	0,8	8	6	0,4	4
N_2 flow [l/h]	0	0	0	4,6	3
Total flow rate [l/h]	20	20	13	14,6	13
pH_2O	4	40	90	2,7	30
Current [A]	6,42	6,42	-6,42	3,18	3,18
Fuel utilization	~ 14%	~ 22%	~ 22%	~ 14%	~ 22%

2.5.6. Presentation and quantification of the degradation at nominal conditions and under stress test

Table 11 **Calculation of the degradation rate**

Degradation rate[1]	$\mathrm{DR}/\%/kh = \frac{(\mathrm{ASR}_{aged} - \mathrm{ASR}_{\mathrm{ref}})}{\mathrm{ASR}_{\mathrm{ref}}} 100 \cdot \frac{1000}{t_{aging}}$ $\mathrm{DR}/m\Omega cm2/kh = (\mathrm{ASR}_{aged} - \mathrm{ASR}_{\mathrm{ref}}) \cdot \frac{1000}{t_{aging}}$ [1]ASR is also computed separately as ohmic and polarisation resistances obtained from the EIS measurements.

For the quantification of the degradation, the cell resistances were computed from *i-V* curves as well as EIS measurements. However, the EIS measurements were chosen for a more detailed comparison to understand the changes observed in the different degradation contributions.

2.5.7. Description of the AST procedure

The sample was tested as per the protocol conditions defined within the consortium in the following steps:

- Heat up under N_2 on the fuel electrode and Air at the air electrode up to desired temperature of 750°C (ASC) and 850°C (ESC).
- Shift to safety H_2 for two hours and then to pure H_2 for 1 hour to ensure complete reduction of the fuel electrode.
- Perform characterisation of the cell using IV curves and EIS spectra at specified fingerprint conditions, i.e. 96/4 H_2/H_2O, 80/20 H_2/H_2O, 50/50 H_2/H_2O with air and O_2 at different temperatures.
- Set specified fuel compositions and perform EIS at regular intervals of 8 h for 1000 h durability operation.
- Cool down as per protocol using safety H_2 and air at air electrode.
- Perform post mortem analysis with SEM.

Table 12 summarises the protocol for the different parameters used in the *in-situ* aging tests for the fuel electrode with different hydrogen/steam ratios to study the effect of steam.

Table 12 **Protocol for ASC and ESC - *in-situ* cell 'steam' fuel electrode aging (DTU).**

	Test input parameters		Comments
steam- approach	temperature	750°C (ASC basis) 850°C (ESC basis)	
	pressure	ambient	
	fuel	60/40 H_2/H_2O **ASC basis** 10/90 H2/H2O **ASC basis** 60/40 H_2/H_2O **ESC basis**	For ASC 10/90 H_2/H_2O was also chosen for further comparison under EC operation conditions.
	oxidant	$f_{air,pos,in}$ x = 178,5 mmol/h/cm^2	
	current density	j = 0,4 A/cm^2 (ASC basis) j = 0,2 A/cm^2 (ESC basis)	

2.5.8. Correlation of the long-term degradation at nominal operation conditions with the degradation at accelerated stress conditions

Anode supported cells

For the Anode supported cells (or fuel electrode supported cells), the different cells that were aged in-situ as per the protocols are summarised in Table 13. It shows the start and end voltages and the degradation rates. The voltage evolution is shown in Figure 9.

Table 13 **Voltage evolution of the in situ operated ASCs under different operation conditions over 1000 h.**

	Inlet fuel composition [mol/mol]	Start voltage [mV]	End Voltage [mV]	Time [h]	Difference [mV kh-1]	Fuel utilization [%]	Percent change [% kh^{-1}]
96/4 FC	87/13	885,77	879,98	1029,60	5,62	~ 14	0,63
60/40 FC	55/45	846,28	831,51	1011,59	14,60	~ 22	1,73
10/90 EC	8/92	995,63	1025,49	1000,05	29,86	~ 22	2,99

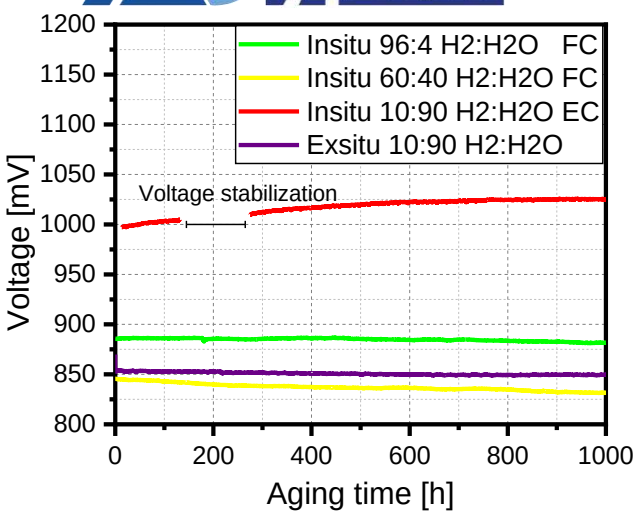

Figure 9 **Voltage evolution over time for ASCs operated at 750°C using air on the air electrode and 96/4 H_2/H_2O at 0,4 A/cm² FC (green), 60/40 H_2/H_2O at 0,4 A/cm² FC (yellow), 10/90 H_2/H_2O at - 0,4 A/cm² EC (red), and aged in 10/90 H_2/H_2O under OCV (ex situ: purple). On the red curve, the voltage stabilization period was after a power outage that occurred.**

Table 14 summarises the different loss contributions for the two cell configurations deconvoluted from EIS measurements. The different frequencies for the contributions are indicated for further understanding of the degradation observed.

Table 14 Summary of the loss contributions in the different cell configurations (ASC and ESC) identified using gas shift EIS measurements.

Loss contributions	ASC	ESC
Fuel electrode		
Gas conversion	~ 1 Hz **(P1)**	
Gas diffusion	30 - 50 Hz **(P2)**	
Charge transfer	2 - 6 kHz **(P4)**	0,1 - 1 Hz **(P1)**
Air electrode		
Gas bulk diffusion	0,3 - 10 Hz **(P2)**	0,1 -10 Hz **(P2)**
$O^{=}$ diffusion and O_2 surface kinetics	0,1 - 1 kHz **(P3)**	0,1 - 1 kHz **(P3)**

Figure 10 indicates that the rate of increase of Rs is highest for the cell operated with 40 % steam under FC mode (Figure 10b) with close to 20 mΩcm²/kh, followed by the cells operated with 90 % steam under EC mode with ca. 6 mΩcm²/kh (Figure 10c) and the cell operated in fuel cell under more dry conditions with ca. 4,5 mΩcm²/kh (Figure 10a), i.e. with rather similar Rs degradation rates. Thus, the ohmic resistance does not show any clear dependency on the operation mode or the fuel compositions for the durability testing. A significant contribution was only observed in

case of the 40 % steam inlet composition FC operated cell, which could also partly arise from the different contact layer on the fuel electrode (fixed channels) used in the test house.

Figure 10 a-c reveal a degradation of the high frequency (~ 1 kHz) contribution, which has been previously identified to be the charge transfer contributions at the fuel electrode. Furthermore, the contribution from the fuel electrode TPB at high frequencies is lower with the increase in steam composition (see Figure 10 a and b) highlighting the favourable reaction kinetics under high steam conditions. The fuel conversion and diffusion contributions were identified at ~ 1Hz for the FC operated cells, whereas in case of the EC with significantly higher steam at the inlet of 90 %, the peak was observed to shift to the lower frequencies and also to be higher in the Bode plots (Figure 10c). This would be a result of the larger effects of diffusion contributions due to the larger size of H_2O molecules as compared to H_2. At the 10/90 H_2/H_2O EC operation (see Figure 10c) due to the applied cathodic overpotential the initial resistance at the high frequencies was higher. However, it must be noted that unlike the comparison of ohmic resistances under the different operation conditions (at same temperature), polarization resistances must be compared at similar conditions (current density) due to dependency of reaction kinetics on the effective fuel composition.

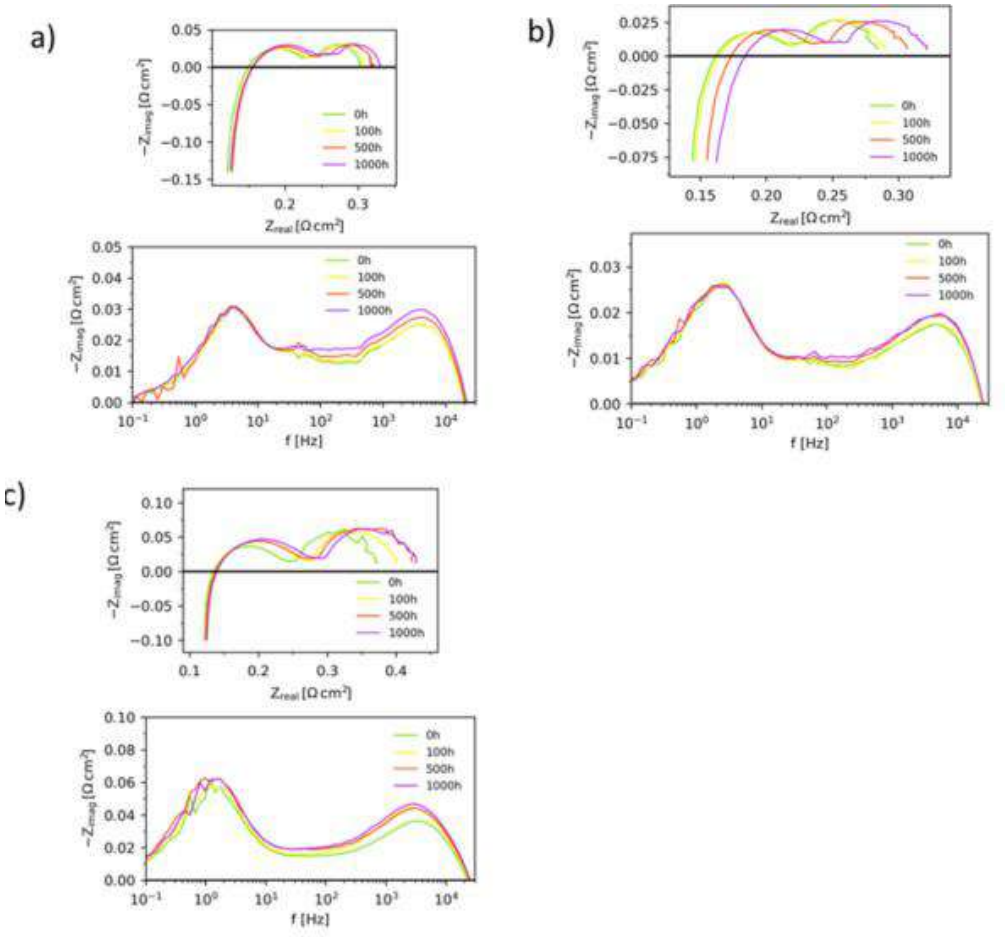

Figure 10 **Nyquist (top) and Bode plots (below) spectra recorded under long term aging at 0 h, 100 h, 500 h and 1000 h for a) 96/4 H_2/H_2O 0,4 A/cm² FC; b) 60/40 H_2/H_2O 0,4 A/cm² FC; c) 10/90 H_2/H_2O – 0,4 A/cm² EC.**

It is crucial to assign a specific frequency region for the changes of the polarization resistance. It is important to understand if the different operating conditions affected the same cell processes without inducing new degradation mechanisms. The pre- and post-test fingerprints for different aging tests were compared at 80/20 H_2/H_2O and air at 750°C. The Bode and DRT deconvolutions for the fuel cell operated cells at high and low steam contents (4 % and 40 %) are shown in Figure 11 a-b respectively. The peaks labelled P1 to P4 have been summarized in Table 14. In case of the 96/4 H_2/H_2O FC operated cell (Figure 11a), an increase was observed at the low frequency region below 1 Hz (P1) which could indicate an increase in the gas conversion contributions. This result, coupled with a higher ohmic resistance of 0,15 Ω.cm^2 at initial fingerprints compared to the 0,13 Ω.cm^2 post durability fingerprints could be associated with non-ideal contact at the initial few hours of the fingerprint measurements (although with good gas sealing throughout). A negligible change was observed at the high frequency ~ 1 kHz associated to the Ni-YSZ charge transfer losses. The peak became more narrow and steeper and thus the area under the peak for DRT deconvolution remained unchanged. For the FC operated cell, with the higher steam content of 40 % (Figure 11b), degradation at the peaks P3 and P4 was observed. A higher variation was observed at P4 associated with the Ni-TPB contributions. The presence of steam has been shown to accelerate the Ni migration in FC operation. This would result in such an increase of the charge transfer contributions. Changes at the air electrode in terms of demixing and degradation in reaction kinetics over long term operation could result in the increase observed at P3 associated to the oxygen surface kinetics. Thus, the fuel cell operation over 1000 h leads to degradation of both electrodes of the ASC.

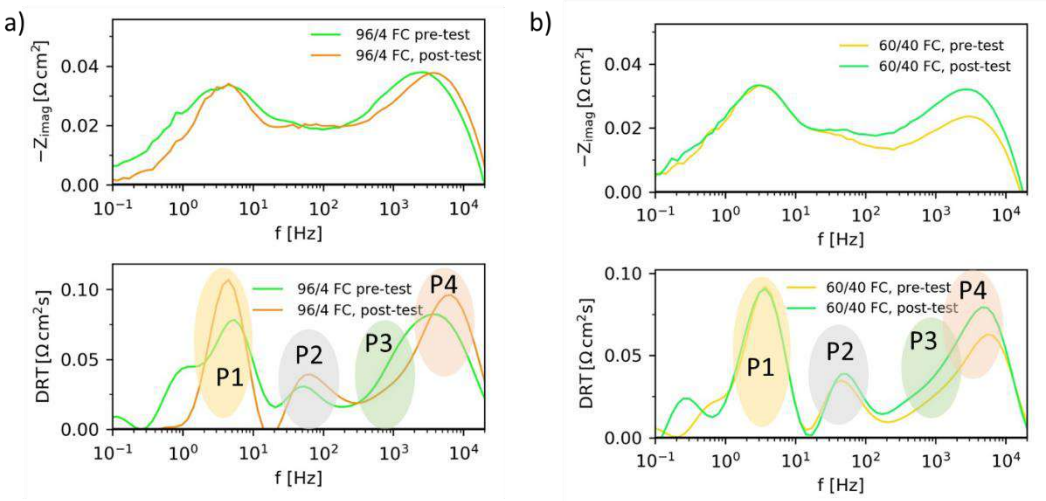

Figure 11 **Bode and DRT plots (top, and bottom) for EIS recorded pre and post durability testing at 750°C with 80/20 H_2/H_2O at OCV for cell operated at a) 96/4 H_2/H_2O composition with 0,4 A/cm^2, FC for 1000 h; b) 60/40 H_2/H_2O composition with 0,4 A/cm^2, FC for 1000 h.**

EIS spectra recorded prior to and post cell operation as electrolysis cell at 10/90 H_2/H_2O inlet fuel composition for 1000 h at - 0,4 A/cm^2 are shown in Figure 12. The ohmic resistances did not change significantly as a consequence of the durability operation. Looking at the polarization resistances, the contributions at the low frequencies are fairly unchanged before and after durability operation. The most significant changes are observed at the middle and high frequency (> 200 Hz) region similar

to the 60/40 FC operated cell. The associated migration and coarsening effects need to be confirmed with microstructural analysis, which is not within the scope of this work.

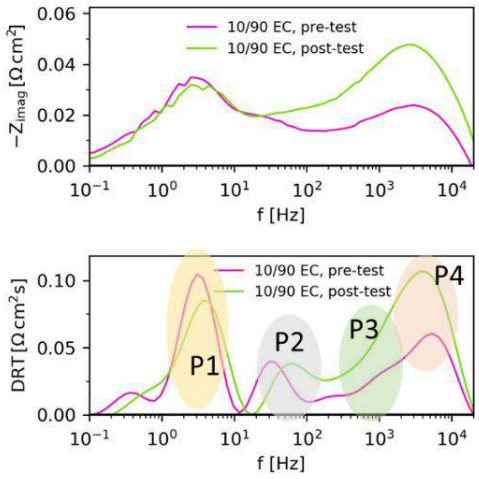

Figure 12 **Bode and DRT plots (top, and bottom) for EIS recorded pre and post durability testing at 750°C with 80/20 H_2/H_2O at OCV for cell operated at 10/90 H_2/H_2O composition with 0,4 A/cm², EC for 1000 h.**

The variation in the air electrode contributions were within 1 % and thus the changes observed at peak P3 in the Bode and DRT plots were a possible consequence of overlapping effects from the variations in Peak P4. As explained earlier the 96/4 FC operated cell has a higher initial resistance as compared to the other aged cells. However, the variation observed at the Ni-TPB contributions pre and post durability operation was negligible. In case of the other three cells, that were aged under 60/40 under FC, 10/90 under EC, the initial charge transfer resistance was comparable. The EC operation showed the highest increase close to 100 % (0,057 Ω.cm2). A charge transfer resistance increase of ~ 71 % (0,038 Ω.cm2) was observed for the FC operated cell with 40 % steam. This further confirms that the presence of high steam accounts for the primary mechanism of the degradation leading to the increase in the charge transfer contribution in ASC configuration with Ni-YSZ fuel electrodes.

Electrolyte supported cells

The effect of operating modes (FC, EC or ex situ under OCV), operating temperature and steam content on the durability behavior of ESCs was studied. The aging conditions over 1000 h are listed in Table 15. Figure 13 shows the cell voltage over operating time for the different cells.

Table 15 **Voltage evolution of the in situ operated ESCs under different operation conditions over 1000h.**

	Actual inlet composition [mol/mol]	Start voltage [mV]	End voltage [mV]	Time [h]	Fuel utilization [%]	Voltage difference [mV/kh]	% voltage change [V%/kh]
96/4 FC	93/7	918,43	912,93	888,62	~ 14	6,19	0,67
60/40 FC	57/43	824,57	812,18	999,50	~ 22	12,39	1,50
60/40 EC	55/45	1031,97	1036,00	1052,00	~ 33	3,83	0,37

60/40 EC High Uf	52/48	1055,77	1064,08	1032,48	~ 83	8,05	0,76

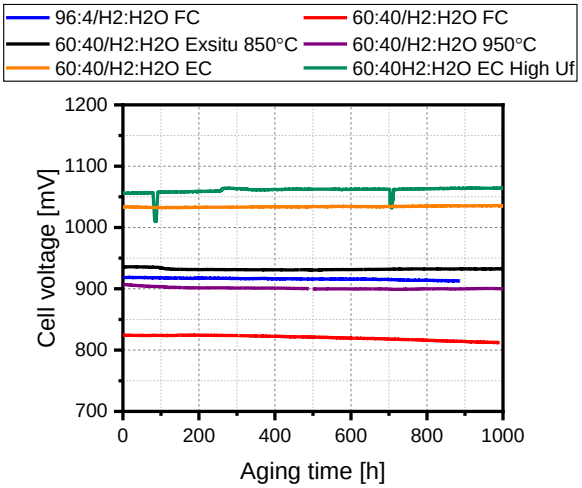

Figure 13 **Voltage Evolution over time for ESCs operated at 850°C using air on the air electrode using 96:4 H_2/H_2O at 0,2 A/cm² FC (blue) ,60/40 H_2/H_2O at 0,2 A/cm² FC (red) , 60/40 H_2/H_2O at - 0,2 A/cm² EC (orange), 60/40 H_2/H_2O at - 0,2 A/cm² EC under high Uf of ~ 83% (green), 60/40 H_2/H_2O at 850°C under OCV (black) and 60/40 H_2/H_2O at 950°C under OCV (purple).**

The voltage drop in case of the 60/40 FC operated cell at a rate of 12,39 mV/kh (1,5 V%.kh^{-1}) is twice the drop observed in case of the FC operation aged under lower steam content, which showed a voltage degradation of 6,19 mV/kh (0,67 V%.kh^{-1}). In case of the EC operation under similar inlet fuel compositions, the voltage rise corresponded to a change of ~ 4 mV/kh (0,37 V%.kh^{-1}) and under a higher fuel utilization it resulted in a difference 2 times higher (than the EC under lower fuel utilization) at 8,05 mV/kh (0,76 V%.kh^{-1}). The post-test OCV values were compared for the different cells and no significant increase in leaks were observed. Thus the cells need to be further studied under similar conditions at OCV for a clear understanding of the variations and to deconvoluted the different loss contributions.

A closer look at the overall cell performance was done by plotting the Nyquist and Bode plots to understand the variation observed in the ohmic and total polarization contributions (see Figure 14 a-d). The ohmic resistances of the four cells under in-situ cells under polarization as fuel cells and electrolysis showed a minor increase over the 1000 h operation. In case of the high steam content in hydrogen, there was a slight increase after ca. 800 h, with a rate of ca. 13 mΩcm^2/kh^{-1} (~ 3,4 %kh^{-1}). In case of the EC operated cell (see Figure 14d), slight increase in ohmic resistance was observed after a H_2 cut off for a few hours close to 85 h into the long term operation resulting in a change at a rate of ~ 14 mΩcm^2/kh^{-1} (~ 5,2 %.kh^{-1}). In case of the 96/4 H_2/H_2O FC operation as well as the EC operation under high fuel utilization, Uf, the low frequency peak was observed ~ 0,2 Hz.

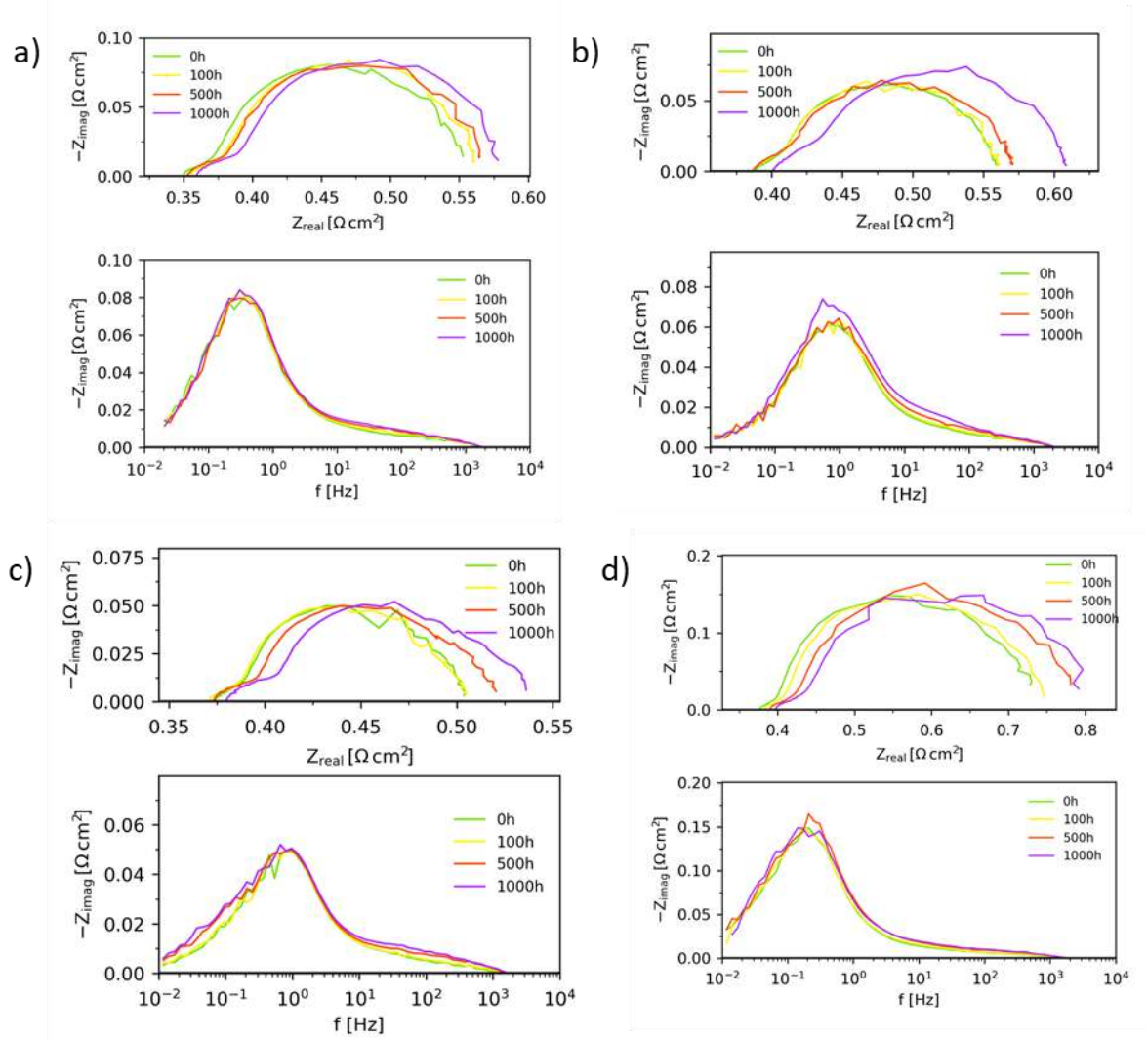

Figure 14 **Nyquist (top) and Bode plots (below) spectra for ESCs under long term aging recorded at 0 h, 100 h, 500 h and 1000 h for a) 96/4 H_2/H_2O 0,2 A/cm² FC; b) 60/40 H_2/H_2O 0,2 A/cm² FC; c) 10/90 H_2/H_2O - 0,2 A/cm² EC; d) 60/40 H_2/H_2O - 0,2 A/cm² EC with ~ 30 % Uf and d) 60/40 H_2/H_2O - 0,2 A/cm² EC with ~ 80 % Uf. (Inductance was vertical and thus not shown for better image ratios).**

The results for the cells operated in FC mode at 0,2 A/cm² and 96/4 and 60/40 H_2/H_2O are shown in **Errore. L'origine riferimento non è stata trovata.**a,b. The cells experience degradation in two different processes, namely at low frequency polarization resistance assigned to the charge transfer resistances and diffusion terms (~ 1 Hz) and at a frequency close to 100 Hz which indicates changes in the oxygen electrode.

However, the changes at the air electrode occur to a much lesser extent in comparison to the fuel electrode losses. The FC aged cell under 60/40 composition showed a higher initial charge transfer contribution (Peak P1) due to some power disruption observed during fingerprint measurements under load prior to the durability testing. These shown initial fingerprints were recorded after resolution of the observed issues. The increase in the polarisation contributions correspond to 24,8 mΩcm²/kh and 38,04 mΩcm²/kh (~ 30% higher) for the FC operated cell under dry and wet inlet conditions respectively. Due to the significant overlap of losses, as previously reported in literature,

the deconvolution of losses in the charge transfer, fuel conversion and diffusion contributions is a challenge.

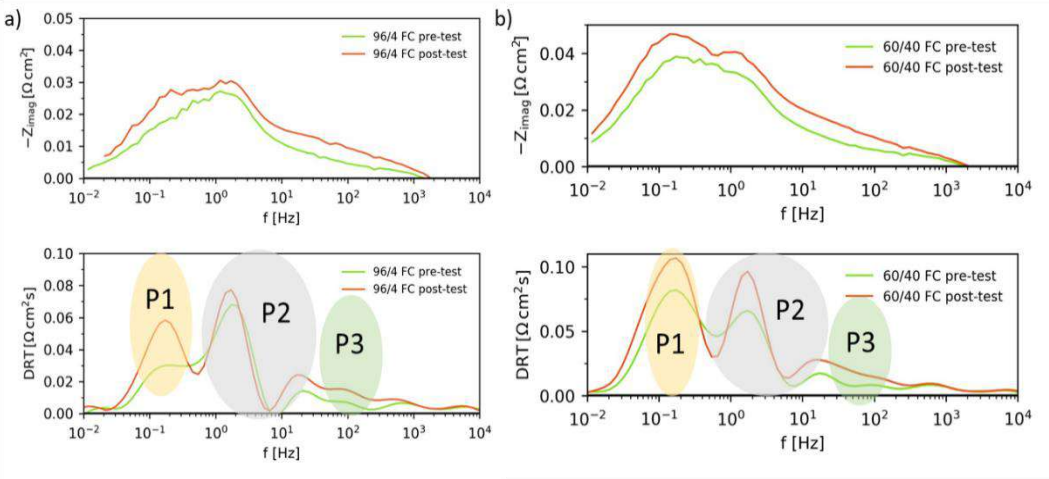

Figure 15 **Bode and DRT plots (top, and bottom) for EIS recorded pre and post durability testing at 850°C with 80/20 H_2/H_2O and air at OCV for cell operated at a) 96/4 H2/H_2O composition with 0,2 A/cm², FC for 1000 h; b) 60/40 H_2/H_2O composition with 0,2 A/cm², FC for 1000 h.**

The pre- and post-durability fingerprints recorded for cells tested under EC operation with 60/40 H_2/H_2O fuel composition and air at air electrode for 1000 h are shown in Figure 16 a and b, respectively. It was observed that the changes in case of the EC operation were primarily at even lower frequencies of ~ 0,1 Hz and no changes were observed at Peak P2 in case of both the EC operated cells. The slight variations at the middle frequency attributed to the air electrode (Peak P3) were observed also in case of the EC operation. The polarisation resistance increase was to a similar extent as compared to the FC operation and the overall contribution of the air electrode remains small. Both EC operated cells showed an increase of ~ 36-37 mΩcm²/kh similar to the 60/40 FC operated cell. Thus, in case of both the FC as well as the EC operation, the increase in polarisation contributions occurred to the same extent. Thus, the operation mode did not contribute significantly to the degradation at these fuel utilization ranges. Although, with a higher inlet steam composition (compared to the 96/4 H_2/H_2O inlet composition), the polarisation resistances showed up to ~ 13-14 mΩcm²kh higher degradation rate at the measured fingerprint conditions.

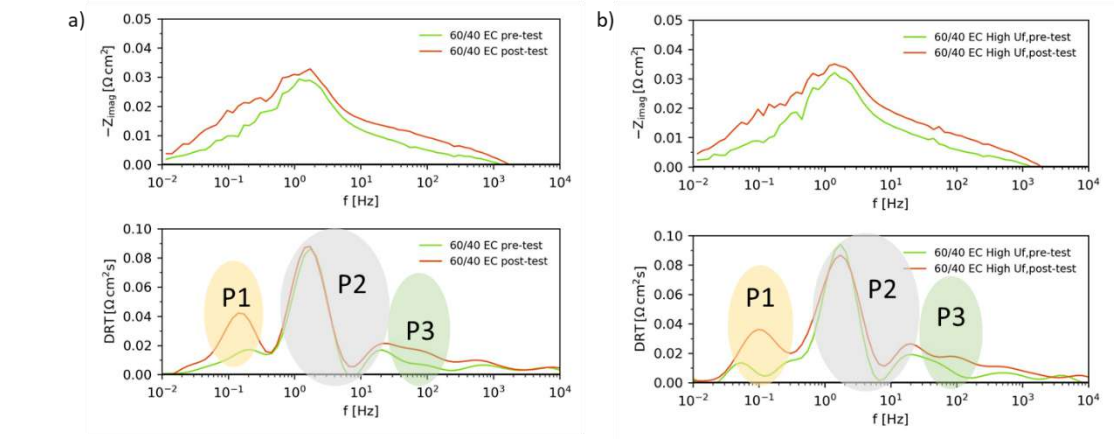

Figure 16 **Bode and DRT plots (top, and bottom) for EIS recorded pre and post durability testing at 850°C with 80/20 H_2/H_2O at OCV for cell operated at a) 60/40 H_2/H_2O composition with - 0,2 A/cm^2, EC for 1000 h; b) 60/40 H_2/H_2O composition with - 0,2 A/cm^2, EC under high fuel utilization for 1000 h.**

2.6. 10-ESC short stack – *in-situ* 'overpotential' aging (EIFER)

2.6.1. Description of the AST Approach

The impact of the current density has been identified as a stressor for the accelerated stress test. The increase of the current density above the nominal operating point is expected to accelerate the degradation of the stack performance. Indeed, the temperature increase induced by the increase of the current density will degrade the stack components like sealing material, interconnect, and cells. As a consequence, the AST protocol for *in-situ* 'overpotential' aging is controlled by the current density and the core temperature of the stack.

2.6.2. Experimental samples

The protocol has been defined and applied on a 10-ESC short stack from Sunfire GmbH. The cells are electrolyte supported cells based on 3 YSZ (90 m) electrolyte with the following architecture: Ni-GDC//GDC//3YSZ//GDC//LSCF where Ni-GDC is the hydrogen electrode, LSCF the oxygen electrode and the GDC layer at the hydrogen electrode side a contact layer while at the oxygen electrode side it is a barrier layer. The samples names are 0054_EIFER_New and 0055_EIFER_New.

2.6.3. Experimental set-up

A commercial test station was used for the operation of the stack. The test station is equipped with oven, gas inlet and outlet process unit as well as control units. The electronic load and the power supply of the test station were adapted for the short stack power for nominal operation and for high-current density operation.

2.6.4. Nominal operation parameters

Table 16 **Nominal operation parameters.**

Sample type	Operation Mode	Parameter	Units	Value	Remarks
Electrolyte supported cells 10 identical cells Short-stack mounted within a hot box	Electrolysis	Temperature	°C	850	
		Pressure	atm	1	
		Fuel	H_2 in Nl/min H_2O in g/min	H_2 = 0,62 H_2O = 4,48	
		Water	% in respect to the fuel	90	
		Air	Nl/min	13,30	
		Current Density	A/cm^2	- 0,5	
		Steam conversion	%	80	
		Oxidant Utilization	%	Non-applicable	
		Other depending on the protocol		Non-applicable	

2.6.5. Stressor (stress parameter) and stress factor

The stress parameter was the current density that has been increased from nominal value by a stress factor of 1,3. The current density has been increased from j = - 0,5 A/cm^2 to j = - 0,65 A/cm^2. The targeted valued of j = - 0,9 A/cm^2 has been hindered by the maximum core temperature of the stack of 860°C above which the sealing material melt.

2.6.6. Presentation and quantification of the degradation at nominal conditions and under stress test

The degradation rate of the stack has been evaluated by estimating the raw voltage degradation and the degradation induced by the temperature increase. Indeed, the stack degradation is described by a voltage increase and an increase of the temperature with the time. Therefore, a temperature-voltage calibration curve is necessary to assess the impact of the temperature on the cell voltage.

Table 17 **Results on the batch tested for high current density**

Degradation rate	Nominal condition	Stress factor: current density
$\mathrm{DR}/\% = \frac{\left(U_{cell}^{aged} - U_{cell}^{t=0}\right)}{U_{cell}^{t=0}} 100 \cdot \frac{1000}{t_{aging}}$ *(1)*	1,3 %.kh^{-1}	Steady state testing was hindered by the Tcore increase above 860°C

(1) Cell voltage measured as a function of time; degradation rate was evaluated using stable operation phase in electrolysis mode for a total of t = 2000 hours for nominal

operation; for high current density, only t = 350 hours operation was available due to the maximum core temperature of 860°C that was reached after this time.

2.6.7. Description of the AST procedure

The operation of the stack in electrolysis mode under nominal operation and under accelerated stress conditions was made with a 10-ESC short stack. The cells were reduced and integrated within a test-box equipped with gas inlet and outlet pipes as well as thermocouples and voltage sense wires.

1) Preliminary diagnosis of the state of the stack and heat-up phase

   The stack is integrated within the test station and an initial gas leakage test is performed at room temperature. Once no leakage has been detected, a compression load of 1200 N is applied and the stack is heated up to 850°C under gas inlet of 60/40 H_2/N_2 at 80 % fuel utilization which implies flow rate of H_2 = 0,19 Nl/min / N_2 = 3,58 Nl/min / Air = 14,37 Nl/min. The cell voltages should be uniform among all the cells and the lateral/vertical temperature gradient of the stack minimized. Thereafter, an electrochemical leakage test is performed to check that the cell voltages drop is within the operation limit once all the gases are switched off.

2) Stack performance in SOFC operation

   If the first phase described above is validated, the stack temperature is increased to 860°C. After stabilization, the current is increased to 26 A and the cell is operated for 100 hours in fuel cell mode to check the performance of the stack. An IV curve was performed under dynamic conditions.

3) Durability test in electrolysis mode under nominal and under high current density

   Thereafter, the durability test in electrolysis mode was started by changing the stack temperature 830°C and the composition of the gas inlets to 90/10 H_2O/H_2 at 80 % steam conversion with the following flow rates H_2 = 0,62 Nl/min/ H_2O = 4,48 g/min / air = 13,30 Nl/min. Once the gases are stabilized the current is increased to - 64 A with a step of 0,5 A/min. The thermoneutral point of 1,3 V is targeted for a core temperature between 820 and 830°C depending on the stack integration. The stack is then operated for 2000 hours without taking into account the failure of components and thus the maintenance time. Finally, the current is increased by 3 A every 48 hours to regulate the core temperature and to keep it below 860°C.

2.6.8. Correlation of the long-term degradation at nominal operation conditions with the degradation at accelerated stress conditions

Stress factor on current density: the correlation can be simply related to the acceleration factor in terms of timing (t) for the degradation on the cell voltage

$$\mathrm{AF} = \frac{t_{long\ term\ test}}{t_{AST\ bringing\ to\ the\ same\ degradation}} = 10$$

Stress factor on current density: the increase of the core temperature accelerates the degradation of the materials like sealings, contact, interconnect and cells.

2.6.9. Annex *(with illustrations* for demonstration of the AST Protocol performance

a) Samples

The architecture of the cells was Ni-GDC//GDC//3YSZ//GDC//LSCF where Ni-GDC is the hydrogen electrode, 3 YSZ (90 µm) the electrolyte and LSCF the oxygen electrode. The GDC layer at the hydrogen electrode side is a contact layer while at the oxygen electrode side it is a barrier layer. Each cell had an active area of 127,8 cm^2. Five thermocouples are distributed along the stack as can be seen in *Figure 17*.b as well five platinum wires where each of them measures the potential difference between two cells defined as cluster.

Figure 17 **Sunfire stack integrated in Eifer test station; b) Schematic drawing of the cells within the stack and the instrumentation.**

(a)

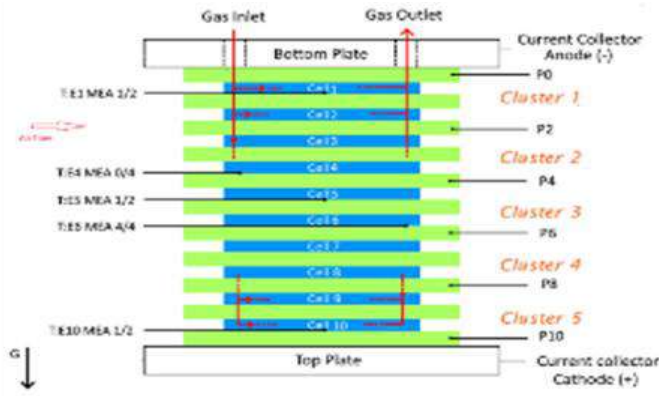

(b)

b) Test set-up

The test station used is a commercial one from Horiba Fuelcon GmbH equipped with the Testwork software that allows a safe semi-automated operation of the stack.

c) Test conditions

The different test phases according to the protocol were applied from the leakage gas test at room temperature to the electrochemical leakage test before switching to fuel cell operation and thereafter electrolysis operation under nominal and high current density.

d) Main results

i-V curve in SOFC and SOEC operation phase

The *i-V* curve, was performed with a scan rate of 0,01 A/s. In order to avoid temperature above 860°C during the acquisition, the oven temperature was decrease to 823°C. As can be seen in Figure 18.c a variation of around 60°C occurs for the core temperature of the stack. A linear fit made in the range of 26 to 36 A indicates an ASR value of 0,787 Ω/cm^2 that is

conform to the expected value. The performance of the stack is characterized by a power density of 0,16 W/cm^2@0,78 V/cell.

The *i-V* curve performed at a scan rate of 0,01 A/s in SOEC mode is shown in Figure 18.d. In this case the core temperature variation is of 30°C with no significant hysteresis. The ASR was estimated with a linear fit to 1,09 Ω/cm^2 at 800°C that is conform to the values for this type of cell at 800°C.

Figure 18 **c) IU curve in SOFC operation; d) IU curve in SOEC mode.**

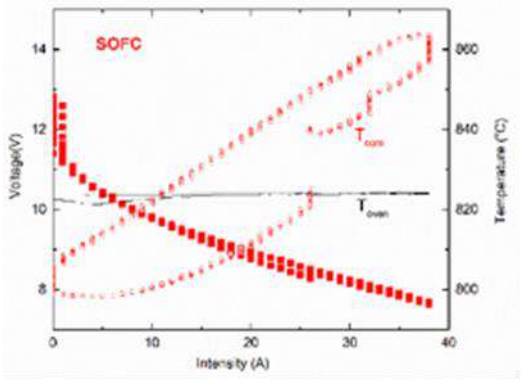

(c)

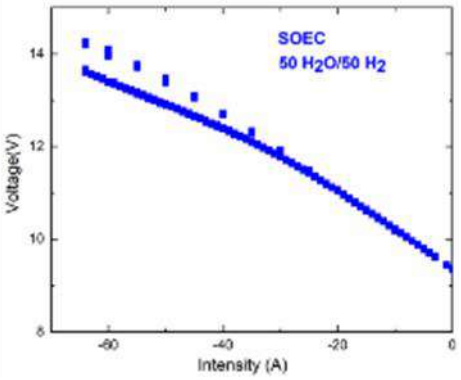

(d)

Durability test phase in electrolysis

The stack has been operated for 2000 hours in electrolysis mode; the operation was not continuous due to several maintenance of components and three stable phases were gathered together to evaluate the degradation. (e) (f)

Figure 19.e displays the time evolution of the voltage and the temperature during these phases. The increase of the voltage and the temperature was analyzed over the 2000 hours of operation and an average degradation rate of 16,6 mV/kh/cell was estimated for the nominal operation under a current density of - 0,5 A/cm^2.

Due to the limitation of the core temperature to 860°C, only - 0,65 A/cm^2 could be reached instead of the target value of - 0,9 A/cm^2. Further, a steady state operation under high current density was also hindered. Figure 19.f displays the high current density operation. As can be seen, the increase in current density increases the cell voltage from an average of 1,45 V/per cell at - 64 A to 1,6 V/cell at - 83 A. All the cluster voltages do not behave similarly with a spread of the voltage between 1,5

and 1,7 V/cell due to the lateral gradient of the temperature of 80°C related to a fault of the preheater. An increase of 3 A corresponds to a voltage increase of around 0,1 V as well as a temperature increase of around 3°C.

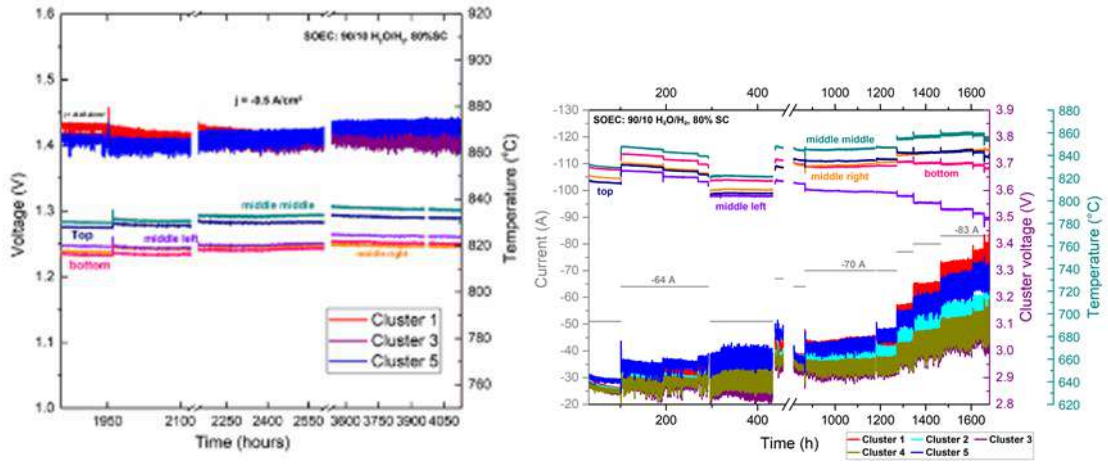

(e) (f)

Figure 19 **e) Evolution of the cluster voltage as well as the temperature as a function of time under 90/10 H_2O/H_2 (steam conversion 80 %) and a current density of j = - 0,5 A/cm². f) Evolution of the cluster voltage as well as the temperature as a function of time under 90/10 H_2O/H_2 (steam conversion 80 %) and by increasing the current density from - 0,5 A/cm² to - 0,65 A/cm².**

Ex-situ **stress test protocols**

2.7. *Ex-situ* interconnect 'Corrosion' aging (EPFL)

2.7.1. Description of the AST Approach

It is of interest to design accelerated ageing tests under harsher than nominal operating conditions, to simulate the long-term (over the whole SOFC lifetime ≈ 40 000 h) ageing behavior at nominal conditions. The operating conditions of the air-side interconnect are simulated in the *ex-situ* test. Based on previous work tasks, temperature and humidity were identified as possible variables for accelerated testing. It is expected that these parameters aggravate the Cr diffusion from the substrate.

2.7.2. Experimental samples

Tests are carried out on both SOLIDpower (SP) and SunFire (SF) coatings. The substrate is ferritic stainless steel K41 with Mn-Cu-Oxide (SP) and Mn-Co-Oxide (SF) protective layers on top. The test area of the samples is 1x1 cm², with an extension on one side to weld contact wires.

2.7.3. Experimental set-up

The ASR test procedure is based on the modified 4-probe testing method (Figure 20). Before running the test, a contact paste of lanthanum strontium cobaltite (LSC) perovskite, is screen-printed on the coated side of the samples and then sintered at 900°C for 6 hours. Basically, the LSC coating is

simulating the interconnect air side and provides the possibility to check Cr-poisoning. The setup configuration is symmetrical which means two identical L-shaped stainless steel/protective coating samples are in contact on the coated side with an LSC layer in between. Lead wires are welded on the arm of the samples and connected to a data logger. Two gold meshes are put on top and bottom of the samples which are connected to a power supply with gold wires. A constant 0,4 A/cm^2 current is passed through the gold meshes and samples. The voltage drop between a sample pair is recorded with the welded wires. Knowing the voltage drop and the current density (0,4 A/cm^2), the ASR is obtained.

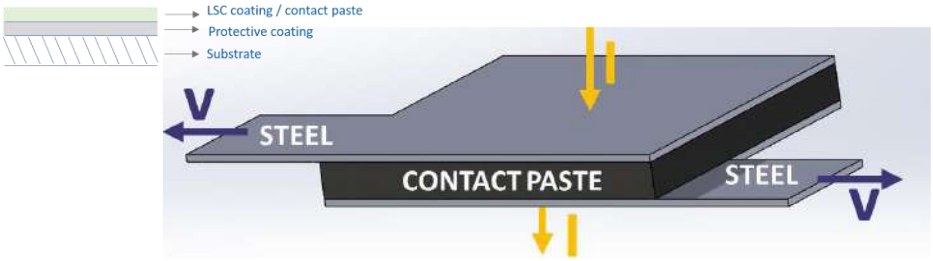

Figure 20 **Schematic of the ASR test configuration.**

2.7.4. Nominal operation parameters

Based on the description of experimental procedure, the following table summarizes the operating parameters of the *ex-situ* ageing test.

Table 18 **Test operating parameters**

Sample type	Parameter	Units	Value	Remarks
IC coating (SF)	Temperature	°C	850, 883, 916, 950	850°C: nominal condition, and the rest are the stressed test temperature. Test temperatures were selected based on design of experiment (DoE).
	Pressure	MPa	0,4	compression
	Humidity	% in respect to the air	15 %	nominal condition: no humidity stressed condition: 15 % humidity.
	Current Density	A/cm^2	0,4	
IC coating (SP)	Temperature	°C	750, 816, 883, 950	Based on DoE, 950°C was removed in the second phase of study (too harsh for this coating material).

	Pressure	MPa	0,4	compression
	Humidity	% in respect to the air	15 %	nominal condition: no humidity stressed condition: 15 % humidity.
	Current Density	A/cm^2	0,4	

2.7.5. Stressor (stress parameter) and stress factor

- Temperature: test temperature was increased from 750-850°C over 950°C,
- Humidity: steam was applied to the test bench as the accelerating factor.

2.7.6. Presentation of the degradation at nominal conditions and under stress test

Results of 1000 hours ageing test results showed that ASR values were constant in nominal and all stressed condition applying higher temperature, and there was no sharp increase in ASR trend. However, the SEM/EDX post-test analysis revealed that Cr thermally grown scale thickness under SF coated samples for the test temperature of 850-950°C is in the range of 1-3,5 µm in dry condition and around 2-7 µm in 15 % RH, but significantly higher under SP coating. For the SP coating at nominal temperature 750°C and dry condition, no continuous Cr oxide layer was found; it formed and grew at higher test temperatures. In dry condition, the scale thickness is on average 3,8, 4,7, and 9,2 µm at temperatures 816°C, 883°C, and 950°C, respectively. In 15 % steam condition, higher Cr thickness (2,6 - 6,2 µm) was observed compared to dry condition. The results are summarized in the following tables.

Table 19 **Results – nominal condition and impact of temperature**

Sample	ASR (nominal condition)	Cr thickness (nominal cond.)	ASR (stressed cond.)	Cr thickness (stressed cond.)
SP coating	< 30 mΩ.cm^2	< 1 µm at 750°C (not continuous)	< 15 mΩ.cm^2 (except for 950°C)	≈ 3,8; 4,7; 9,2 µm (816°C; 816°C; 950°C)
SF coating	< 30 mΩ.cm^2	≈ 1 µm at 850°C	< 15 mΩ.cm^2	≈ 1,5-3,5 µm

Table 20 **Results – nominal condition and impact of humidity**

Sample	ASR (nominal condition)	Cr thickness (nominal cond.)	ASR (stressed cond.)	Cr thickness (stressed cond.)
SP coating	< 30 mΩ.cm^2	< 1 µm at 750°C (not continuous)	< 30 mΩ.cm^2	≈ 2,6 µm (at 750°C; 15% RH)
SF coating	< 30 mΩ.cm^2	≈ 1 µm at 850°C	< 30 mΩ.cm^2	≈ 2,1 µm (at 850°C; 15% RH)

Table 21 **Results – nominal condition and impact of humidity + temperature**

Sample	ASR (nominal condition)	Cr thickness (nominal cond.)	ASR (stressed cond.)	Cr thickness (stressed cond.)
SP coating	< 30 mΩ.cm^2	< 1 µm at 750°C (w/o humidity)	< 30 mΩ.cm^2	≈ 2,6 – 6,2 µm (at 750°C-883°C; 15 % RH)
SF coating	< 30 mΩ.cm^2	≈ 1 µm at 850°C (w/o humidity)	< 30 mΩ.cm^2	≈ 2,1 - 7 µm (at 850°C-950°C; 15 % RH)

2.7.7. Quantification (measurement) of the degradation

In IC corrosion ageing test, ASR value/trend and Cr thickness show the degradation level. The quantification for the tested samples summarized in above tables (section 2.7.6).

2.7.8. Description of the procedure

Experimental procedure and operating parameters are described in 2.7.3 and 2.7.4 sections. Tests are run for 1000 hours at operating temperatures between 750-950°C and the ASR value recorded every 5-minutes during the whole test time. After the tests, samples are analyzed by SEM/EDX for Cr diffusion.

2.7.9. Correlation of the long-term degradation at nominal operation conditions with the degradation at accelerated stress conditions

The accelerated tested samples can be correlated to the long-term tested samples in standard conditions mainly by comparing the Cr thickness and Cr diffusion percentage through the coating. In the earlier stages of the project, SEM/EDX post-test analysis was performed on SF long-term tested samples (aged for 2Kh, 5kh, 9kh, 15kh, 20kh, and 40kh) and Cr scale thickness was measured. Based on the result comparison, considering SF long-term aged IC on the airside and outlet, it was found that :

- temperature as the accelerating factor in the harshest condition (T=950degC) can be correlated to the standard test condition aged above 5kh.
- by adding humidity (15%) to the high temperature (950degC) test condition, the accelerating condition can be correlated to the standard test condition aged c.a 9kh.

2.8. *Ex-situ* electrochemical redox cycle aging via O^{2-} (ENEA)

2.8.1. Description of AST approach

The approach aims to induce subsequent oxidation and reduction cycles at the fuel electrode using the O^{2-} ions coming from the electrolyte, in fuel cell mode. This should trigger Ni coarsening and Ni segregation phenomena that are usually observed in long term on-field operated samples, especially at high fuel utilizations. It is supposed to have a major impact at electrode/electrolyte interface, where subsequent Ni redox cycles can also induce localized mechanical stresses due to volume contractions/expansions, leading to the detachment of the fuel electrode from the electrolyte layer.

2.8.2. Experimental samples

Samples employed for this AST approach are ES-SOC half cells, 5x5 cm^2 (4x4 cm^2 active area). Half cells were selected to avoid any contribution of cathode material to the impedance spectra. These samples were used to assess the impact of redox cycles on the fuel electrode and fuel electrode/electrolyte interfaces.

To obtain an estimation of the degradation rate and acceleration factor, as well as verify that the induced mechanisms are representative of on-field operation, child samples coming from complete ES-SOC cells were cut into 2,5x2,5 cm^2 (2x2 cm^2 active area) samples, in order to compare them to similar child samples obtained from available fragments of on-field operated cells.

2.8.3. Experimental set-up

For ES-SOC half cells, the experimental set-up is a simple single cell housing, employing two stainless steel frames for 5x5 cm^2 cells, Ni net as fuel electrode current collector, Pt net as air electrode current collector, two Pt wires as voltage sensors, and two Thermiculite gaskets as sealings for fuel and air compartment.

Since the tested samples are half cells, Pt net also acts as the counter electrode; the Pt wire used as voltage sensor for the counter electrode is placed on the edge of the electrolyte by means of a small amount of Pt contacting paste. A schematic representation of the set-up is depicted in Figure 21.

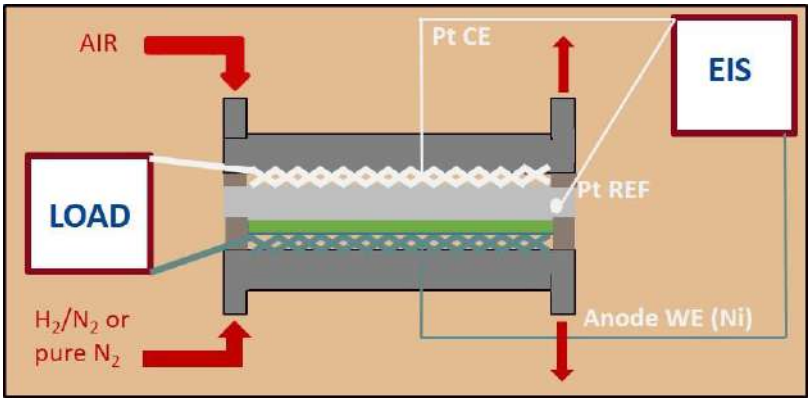

Figure 21 **Schematic representation of the testing set up for electrochemical *ex-situ* redox cycles.**

For child samples coming from complete cells, a button cell test rig was employed, consisting of an alumina support where the cell is held vertically by a high temperature refractory paste, a Ni mesh

and two Ni wires as anode current collector and an Au mesh with two Au wires as cathode current collector. A schematic representation of this set-up is reported in Figure 22.

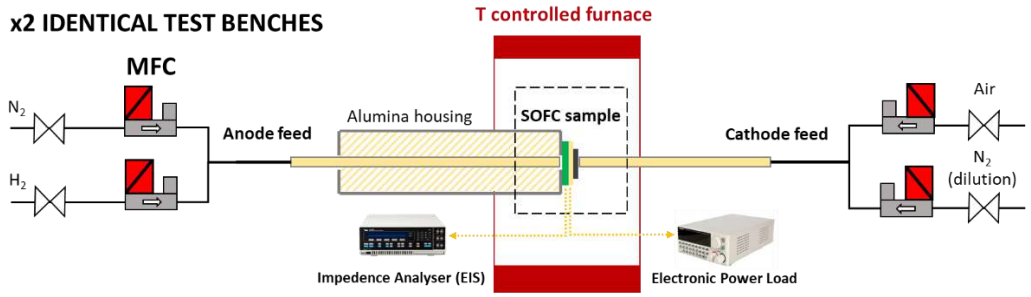

***Figure 22* Schematic representation of the testing set up for *ex-situ* redox cycles.**

2.8.4. Nominal operation parameters

***Table 22* Nominal operation parameters**

Sample type	Operation Mode	Parameter	Units	Value	Remarks
ES-SOC half cell	SOFC	Temprature	°C	850	
		Pressure	bar	1	
		Fuel	Nml/min/cm^2	14,28	H_2/N_2 60/40
		Water	% in respect to the fuel	0	
		Oxidant	Nml/min/cm^2	62,5	Air
		Current Density	A/cm^2	0,05; 0,1; 0,2	Only applied during cycles
		Fuel Utilization	%		
		Oxidant Utilization	%		
		Fuel	Nml/min/cm^2	5,71	N_2 (H_2=0 Nml/min/cm^2) only applied during cycles

2.8.5. Stressor (stress parameter) and stress factor

The stressing agent is the O^{2-} flow from the electrolyte to the fuel electrode in absence of H_2.

Electrochemical cycles are defined by a set of 3 principal stress parameters:

- **$I_{oxidation}$**: current density (A/cm^2) imposed to the cell when the H_2 supply is interrupted,
- **$t_{starvation}$**: duration of the starvation condition (H_2 = 0 ml/min),
- **$V_{threshold}$**: lower cell voltage reached during the starvation period at fixed $I_{oxidation}$.

2.8.6. Presentation and quantification of the degradation at nominal conditions and under

stress tests

ASR is obtained by means of EIS spectra performed after each redox cycle.

Suggested EIS parameters are:

Polarization: OCV or 0,05 A/cm^2,

Amplitude: 0,01 A/cm^2,

Frequency range: from 1.10^5 Hz to 2.10^{-3} Hz,

Number of points: 10 - 12 points/decade.

The degradation rate is very high and largely depends on the selected cycling parameters.

For these redox cycles, the degradation rate has been calculated for 10 redox cycles performed with: $I_{oxidation}$ = 0,05 A/cm^2, $V_{threshold}$ = 0,4 V, $t_{starvation}$ < 1min (depends on $I_{oxidation}$ and $V_{threshold}$). Each cycle is considered to require 5 hours (with EIS included), therefore t_{aging} = 50 h.

The degradation rate for nominal conditions is calculated considering the ASR measured from child samples (see 2.8.8) coming from complete cells operated for 20 000 hours in SOFC mode, therefore t_{aging} = 20 000 h.

Table 23 **Degradation rate results**

Degradation rate	Nominal condition	Stress factor: redox cycles via O^{2-}
$\mathrm{DR}/\% = \frac{\left(ASR_{cell}^{aged} - ASR_{cell}^{t=0}\right)}{ASR_{cell}^{t=0}} 100 \cdot \frac{1000}{t_{aging}}$	2,61 %.kh^{-1}	471,1 %.kh^{-1}

As results from the degradation rate, redox cycles via O^{2-} are very fast and extremely aggressive.

2.8.7. Description of AST procedure

The sample is exposed to a selected number of cycles comprising the following steps:

- Stabilization and OCV measurement at nominal conditions.
- Set current to I=$I_{oxidation}$ and stabilization of the cell voltage.
- Set H_2 = 0 ml/min for a fixed period of time ($t_{starvation}$) or until V_{cell} = $V_{threshold}$.
- Reduction procedure according to manufacturer's specification.
- EIS measurement at nominal conditions.

A schematic overview of the electrochemical cycles is reported in Figure 23.

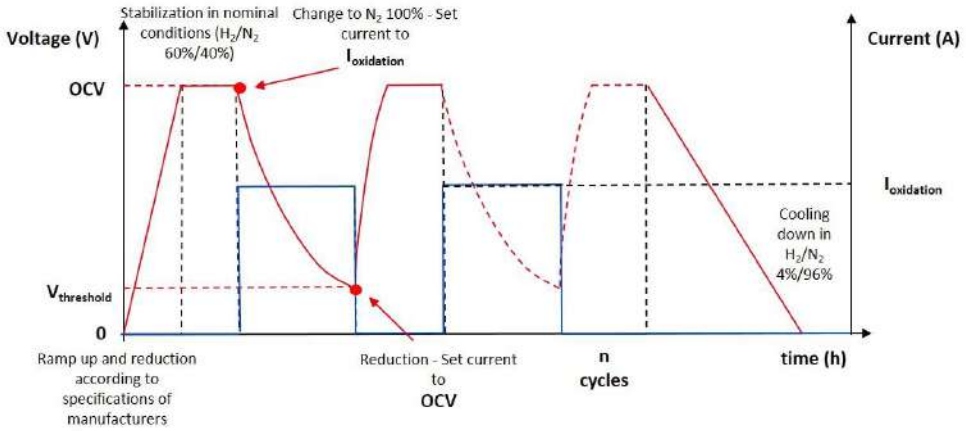

Figure 23 **Schematic overview of electrochemical ex-situ aging experiment.**

The impact of electrochemical redox cycles largely depends on the selection of $\mathbf{I_{oxidation}}$, $\mathbf{V_{threshold}}$ and $\mathbf{t_{starvation}}$.

In Table 24 below, the suggested values result from an extensive experimental campaign where these cycles were performed by setting different combination of the following parameters:

- $\mathbf{I_{oxidation}}$: 0,05 A/cm^2; 0,1 A/cm^2; 0,2 A/cm^2,
- $\mathbf{t_{starvation}}$: < 1 min; 1 min; 10 min,
- $\mathbf{V_{threshold}}$: 0 V; 0,2 V; 0,4 V.

Number of cycles tested were up to 10, but it may vary depending on the selected values of the abovementioned parameters and cell nature.

Table 24 **Test input parameters of electrochemical redox cycles**

	Test input parameters	
Electrochemical redox-cycle	temperature	850°C (ESC basis)
	pressure	Ambient
	fuel	**Dry 60/40 H_2/N_2 ESC basis** $f_{H2,neg,in}$: x = 8,57 Nml/min/cm^2 $f_{N2,neg,in}$: x = 5,71 Nml/min/cm^2 **During redox cycle** $f_{H2,neg,in}$: x = 0 Nml/min/cm^2 $f_{N2,neg,in}$: x = 14,28 Nml/min/cm^2
	oxidant	$f_{air,\ pos,\ in}$: x = 62,5 Nml/min/cm^2
	Current density ($I_{starvation}$ during cycles)	< 0,05 A/cm^2
	Voltage ($V_{threshold}$ during cycles)	0,2 V < $V_{threshold}$ < 0,6
	Time ($t_{starvation}$ during cycles)	< 1 min; depends on $I_{starvation}$ and $V_{threshold}$

	samples	ES-SOC half cells (fuel electrode) or full cells
	Target	SOFC (CHP)
	Post-test characterization	SEM microscopy

2.8.8. Correlation of the long-term degradation at nominal operation conditions with the degradation at accelerated stress conditions

Child samples were cut from cells coming from stacks operated in SOFC mode and provided by the manufacturer. Available samples were operated for 0, 2000, 5000, 15 000 and 20 000 hours.

By an extensive experimental campaign, comprising parametrical process identification, EIS measurements, DRT elaborations and ECM-CNLS fitting calculations, it was possible to extrapolate an estimation of the on-field degradation experienced for the resistance of each physico-chemical process. A linear regression was applied to retrieve an estimation of the degradation rate from the slope of the curves (Figure 24).

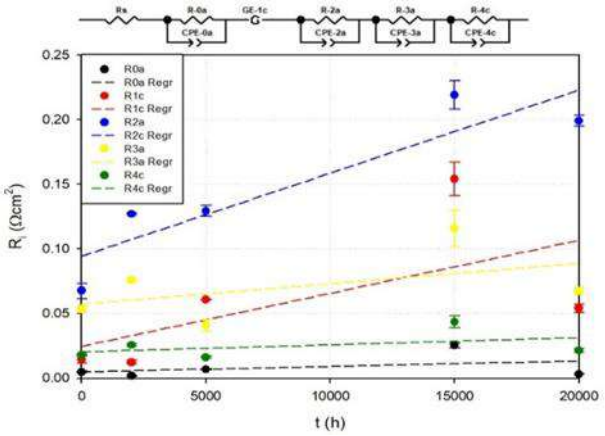

$$R_{0a} = 4{,}27 \cdot 10^{-7} t + 4{,}79 \cdot 10^{-3}$$

$$R_{1c} = 4{,}09 \cdot 10^{-6} t + 0{,}025$$

$$R_{2a} = 6{,}42 \cdot 10^{-6} t + 0{,}094$$

$$R_{3a} = 1{,}58 \cdot 10^{-6} t + 0{,}057$$

$$R_{4c} = 5{,}50 \cdot 10^{-7} t + 0{,}020$$

Figure 24 **Temporal evolution of resistances related to each process in on-field operated samples. The x-axis reports the time that on-field samples were operated in fuel cell mode.**

For 10 redox cycles performed with: $I_{oxidation}$ = 0,05 A/cm^2, $V_{threshold}$ = 0,4 V, $t_{starvation}$ < 1min (depends on $I_{oxidation}$ and $V_{threshold}$), the percentage of degradation obtained on each process, and to the acceleration factor was estimated. Each cycle is considered to require 5 hours (with EIS included), therefore t_{aging} = 50 h. EIS and DRT plots for this sample are reported in Figure 25.

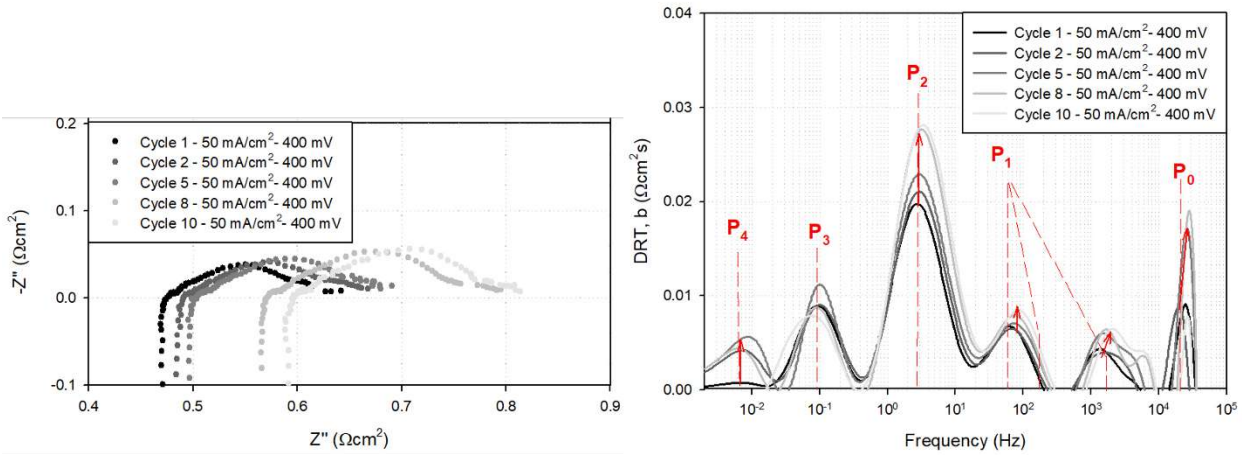

Figure 25 **EIS and DRT spectra of the sample that performed 10 cycles with: $I_{oxidation}$ = 0,05 A/cm², $V_{threshold}$ = 0,4 V, $t_{starvation}$ < 1min.**

By applying a CNLS fitting procedure of the measured impedance spectra with the same ECM depicted in Figure 24, and considering the slopes of the regression lines as an estimation of the degradation rates of each process, it results that:

- R_{0a} increased by 35 %, corresponding to ≈ 8000 hours of SOFC on-field operation,
- R_{1c} increased by 76 %, corresponding to ≈ 5000 hours of SOFC on-field operation,
- R_{2a} increased by 65 %, corresponding to ≈ 6500 hours of SOFC on-field operation,
- R_{3a} increased by 4 %, corresponding to ≈ 1000 hours of SOFC on-field operation,
- R_{4c} increased by 32 %, corresponding to ≈ 2000 hours of SOFC on-field operation.

Depending on the process considered, this corresponds to an acceleration factor of:

$$\mathrm{AF} = \frac{t_{long\ term\ test}}{t_{AST\ bringing\ to\ the\ same\ degradation}} = from\ 20\ to\ 160$$

NOTE: electrochemical redox cycles via O^{2-} are extremely aggressive. They may lead to undesired and non-representative effects, such as structural damages of anode lattice and detachments of electrode layers from the electrolyte, that may ultimately cause cell failure.

2.9. *Ex-situ* ESC half-cell chemical redox cycle aging via O_2 partial pressure (ENEA)

2.9.1. Description of the AST Approach

The AST is based on the concept of performing an *ex-situ* pre-ageing of fuel electrodes of ESC half cells (electrolyte-anode configuration) via chemical redox cycling. The pre-aged fuel electrodes are then shipped to the manufacturer (Sunfire) which applies the oxygen electrode by screen-printing and sintering procedure and the resulting full cell with pre-aged anode is first characterized from an electrochemical point of view (*i-V* curves, EIS before and after a stabilization period under load) and finally sent to post-test image analyses (SEM-EDX).

In this way it is possible to quantitatively assess the degradation effect of the chemical cycling of the fuel electrode (subsequent reduction and oxidations between Ni-NiO) in terms of electrochemical performances and microstructure/morphology.

The results are compared to a pristine cell manufactured with the same procedure (half cell electrolyte-anode + screen printing & sintering) to determine the accelerated phenomena.

Additionally, to better control the pre-aging phase an alternative approach has been explored, using a half cell where, instead of having bare electrolyte at the cathode electrode compartment, a LSM conductive paste has been applied on the electrolyte, aiming to simulate a full cell electrochemical behaviour, and allowing EIS measurements after each cycle.

Finally, the results are correlated to on-field samples to evaluate which are the effects that are induced via the AST that can also be found in on-field samples subject to calendar ageing and to quantitatively determine the AF.

2.9.2. Experimental samples

The protocol is intended for Electrolyte Supported Cell (ESC) half cell samples, cells present a square geometry with a YSZ supporting electrolyte layer (3x3 cm; ≈ 85 µm) and a single 3-layer Ni-CGO fuel electrode (1x1 cm; ≈ 25 µm in reduced phase). The other side of the electrolyte is bare.

Although 4 samples were mounted for each ex-situ chemical pre-ageing test at least 1 cell for each pre-treatment batch has been tested in the electrochemical test bench (due to failures and time and resources limitations).

The half-cell used for the alternative approach of the pre-ageing phase is a square geometry with a YSZ supporting electrolyte layer (5x5 cm; ≈ 85 µm) and a single 3-layer Ni-CGO fuel electrode (4x4 cm; ≈ 25 µm in reduced phase).

2.9.3. Experimental set-up

Since the AST is carried out in two steps (pre-ageing and testing), two different experimental setups are used for the two phases of the experiment, described below.

***Ex-situ* pre-ageing by chemical cycles**

The cells are mounted in a single-cell metallic cell holder, in which a customized sealing geometry is designed to ensure single atmosphere in both sides of the holder. In the specific case of ENEA facilities, the used holder (10x10 cm) can house up to four samples per test (Figure 26).

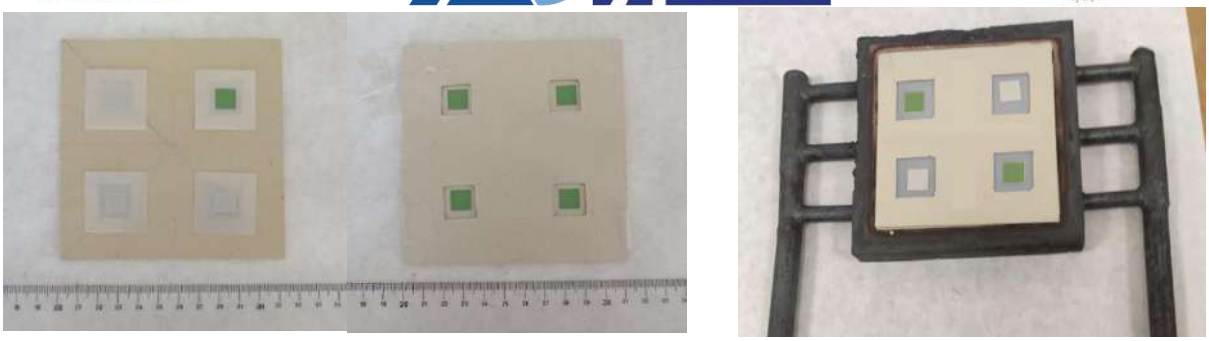

a) b)

Figure 26 **Experimental setup for *ex-situ* artificial pre-ageing of fuel electrodes via redox cycling: a) Custom gas sealing; b) Cell holder configuration.**

The samples were placed in a temperature-controlled furnace which is operated at fixed temperature (850°C, nominal ESC temperature) with ≈ 50 kg applied spring load to contain the volume variations during the phase changes and avoid sealing failure (Figure 27).

The gas distribution system was adapted to provide alternating reducing (H_2 and N_2) and oxidizing (air) atmospheres to all samples by two three-way non-return valves fitted on the inlet/outlet pipes.

The same set-up was used to age the 5x5 cm^2 sample, by employing specific cell manifolds, while the gas distribution provided a homogeneous oxidising atmosphere at the cathode side and alternating reducing/oxidising atmosphere at the anode side, without the necessity of using two three-way non-return valves fitted on the inlet/outlet pipes since the two compartments were intentionally kept isolated in this case.

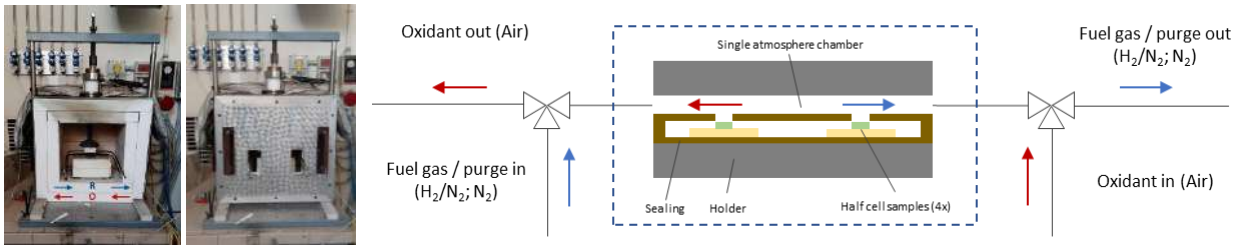

a) b)

Figure 27 **Experimental setup for *ex-situ* artificial pre-ageing of fuel electrodes via redox cycling: a) Test rig configuration; b) Redox cycling procedure scheme.**

Full cell electrochemical characterization

The electrochemical characterization is carried out in a standard ceramic button-cell test setup (see 2.8.3). The gas distribution system supplies gas from external gas bottles, separate Mass Flow Controllers are installed in each line to control the flow rate of the gases to the anode and cathode compartment. The anode and cathode feeds are supplied to the fuel cell sample through alumina ceramic housing, placed inside a temperature-controlled furnace.

The electrical interface is composed of a DC electronic power load and a separate Impedance Analyzer module coupled with an Electrochemical Interface for the Electrochemical Impedance Spectroscopy measurements. The instrumentation is connected to the cell via separate current and

voltage wires, attached to current collector meshes to ensure uniform current distribution (Ni and Au for anode and cathode side). Separate current and voltage wires reduce voltage perturbation from current flow and allow to perform 4-point impedance measurements.

2.9.4. Nominal operation parameters

Also in this case, the nominal operation parameters are divided between the two steps of the experiment.

<u>*Ex-situ* pre-ageing</u>

***Table 25* Nominal Operation parameters (Step 1 - *ex-situ* pre-ageing).**

Sample type	Operation Mode	Parameter	Units	Value	Remarks
		Temprature	°C	850	Nominal temperature ESC
		Pressure	Bar	Ambient	
		Fuel	Nml/min/cm^2	400	25/75% H_2/N_2 reducing 100% N_2 purge
		Water	% in respect to the fuel	0	dry
		Oxidant	Nml/min/cm^2	400	Air
		Current Density	A/cm^2	-	N/A
		Fuel Utilization	%	-	N/A
		Oxidant Utilization	%	-	N/A
		Other depending on the protocol	Reducing (3h) and oxidizing (1h) atmospheres are alternated for n times, separated by purge (1h). Both gases are provided alternatively to the same electrode (anode) – single atmosphere.		
		Other depending on the protocol (alternative ageing procedure)	Reducing (3h) and oxidizing (1h) atmospheres are alternated for n times, separated by purge (1h). The alternance of the atmospheres occurred at the anode side, while the cathode compartment maintained the same oxidising atmosphere for the entire duration of the protocol.		

<u>Full cell electrochemical characterization</u>

Table 26 **Nominal operation parameters (Step 2 – Full cell electrochemical characterization).**

Sample type	Operation Mode	Parameter	Units	Value	Remarks
ESC Full cells (with printed cathode)	Standard SOFC characterization mode	Temprature	°C	850	Nominal temperature ESC
		Pressure	Bar	Ambient	
		Fuel	Nml/min/cm^2	100	60/40 % H_2/N_2
		Water	% in respect to the fuel	0	dry
		Oxidant	Nml/min/cm^2	200	Air
		Current Density	A/cm^2	0,25	100 h stabilization under load (EIS is performed in OCV)
		Fuel Utilization	%	≈ 5 %	Only during stabilization period
		Oxidant Utilization	%	≈ 5 %	Only during stabilization period
		Other depending on the protocol			

2.9.5. Stressor (stress parameter) and stress factor

The chemical redox cycle which causes alternating anode reduction/oxidation between Ni-NiO which represents the stressor. Reducing (3h) and oxidizing (1h) atmospheres are alternated for n cycles, separated by purge (1h). The chemical redox cycle parameters are shown below. The choice of the abundant flow rates and durations is intentional to obtain full reduction/oxidation of the Ni in the anode (Figure 28).

Table 27 **Chemical redox cycle parameters.**

T = 850°C; n= 4; 8; 12 cycles				
		Reduction phase	Purge phase	Oxidation phase
Composition	(% vol.)	25/75 % H_2/N_2 reducing	100 % N_2 purge	100 % Air (21 % O_2) oxidizing
Flow rate	(Nml/min/cm^2)	400	400	400
Duration	(h)	3	1	1

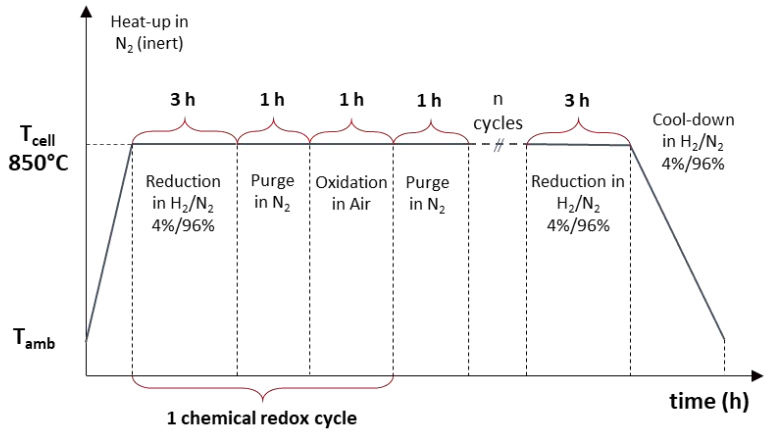

***Figure 28 Ex-situ* pre-ageing chemical redox cycle scheme.**

The main effect of the alternating anode reduction/oxidation between Ni-NiO is related to the volume change (volume variation ΔV/V ≈ 40 %) which could induce µ-cracks, delamination, and mechanical damage to the cell sample. The volume variation could even lead to an increase of the electrode bulk volume, considering that the ceramic backbone remains chemically stable. Also, the Ni particle distribution could vary during subsequent oxidation and reduction phases, without a return to the initial Ni particle distribution.

Typically, such conditions are not desired during normal use (accidental events such as fuel starvation, fuel leakage, improper shut-down procedure), therefore it is foreseen that the chemical redox cycling has an important stress factor respect to calendar aged samples. During regular operation the cells should undergo only one chemical cycle throughout the whole operation time, consisting in the initial reduction of the NiO into Ni, occurring at the first startup. In fact, excluding undesired events, a reducing atmosphere should be always ensured during operation and during controlled standby or shut-down procedure.

2.9.6. Presentation and quantification of the degradation at nominal conditions and under stress test

The degradation rate for nominal conditions is calculated considering the ASR measured from child samples (see 2.8.8) coming from complete cells operated for 20 000 hours in SOFC mode, therefore t_{aging} = 20 000 h.

Each redox cycle is considered to require 5 hours, therefore t_{aging} = 20 h and t_{aging} = 40 h for 4 and 8 cycles, respectively.

***Table 28* Degradation rate results**

Number of cycles	Degradation rate	Nominal condition	Stress factor: redox cycles via O_2
4	$\mathrm{DR}/\% = \frac{\left(ASR_{cell}^{aged} - ASR_{cell}^{t=0}\right)}{ASR_{cell}^{t=0}} 100 \cdot \frac{1000}{t_{aging}}$	2,61 %.kh^{-1}	266,5 %.kh^{-1}

8	$\mathrm{DR}/\% = \frac{\left(ASR_{cell}^{aged} - ASR_{cell}^{t=0}\right)}{ASR_{cell}^{t=0}} 100 \cdot \frac{1000}{t_{aging}}$	2,61 %.kh^{-1}	1621,5 %.kh^{-1}

The quantitative degradation indicators for the AST are represented by difference in the electrochemical results of the full cell with pre-aged anode as a function of n (# of redox cycles) with respect to a pristine cell sample.

- ASR: measured from EIS

The identification of the affected physico-chemical phenomena is obtained by qualitative analysis of the DRT spectra as a function of n (# of chemical cycles) in comparison to the DRT spectra of a pristine sample (full cell). The modifications of the microstructure/morphology observed in the SEM images are evaluated qualitatively, based on visual inspection. Results obtained with 12 cycles aged cells were affected by an abnormal increase in the ohmic resistance caused by a severe detachment of the cathode electrode, thus was not possible to use them for the quantification of the degradation.

2.9.7. Description of the AST procedure

The AST procedure is summarized as follows:

- *Ex-situ* pre-ageing of ESC half cells (electrolyte-anode) – n cycles of alternating reducing and oxidizing atmospheres @ 850°C (n= 4; 8; 12 cycles),
- *Ex-situ* alternative pre-ageing of ESC half cells (anode-electrolyte-LSM paste) - n cycles of alternating reducing and oxidizing atmospheres @ 850°C monitoring continuously the effect of ageing via EIS spectra performed after each cycle,
- Cathode screen printing & sintering by manufacturer → resulting in full cells with pre-aged anodes,
- Electrochemical characterization (IV curves, EIS spectra – t = 0 h),
- Stabilization under current load (j = 0,25 A/cm^2; t = 100 h, when possible),
- Electrochemical characterization (IV curves, EIS spectra – t = 100 h, when possible),
- Post-test characterization (SEM-EDX).

***Figure 29*: schematic description of O_2 redox cycle AST procedure**

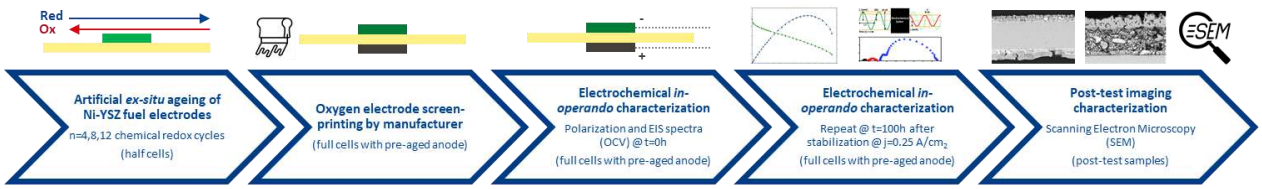

The suggested IV polarization parameters are:	The suggested EIS parameters are:

• Galvanostatic stepwise current sweep • j_{max} = 0,5 A/cm^2 (when possible)	• Potentiostatic in OCV conditions • Amplitude: 0,10 mV • Frequency range: from 1x10^5 Hz to 2x10^{-3} Hz • Number of points: 12 points/decade

A preliminary mapping of the physico-chemical processes is obtained by means of extensive parametric DRT campaign of pristine cells (variation of operating parameters: H_2 vol 10/20/60/90 % vol.; O_2 vol. 2/4/6/21 % vol.; T_{cell} 825/850/875°C).

2.9.8. Correlation of the long-term degradation at nominal operation conditions with the degradation at accelerated stress conditions

From an electrochemical point of view, it is confirmed that the AST affects the anode processes (larger Rpol, increased DRT peaks in the anode processes between 0,01-10 Hz ascribed to anode charge and mass transfer) with increasing severity as a function of n (# of redox cycles).

Likewise, the SEM observations show a variation of Ni particle distribution in all the anode (mainly Ni agglomeration, resulting from Ni migration and subsequent coalescence), which is coherent with the electrochemical performance loss – considering the Ni-CGO material properties in terms of electrochemical behaviour. Semi-quantitiative/quantitative image analysis would be useful to numerically assess the changes in the anode microstructure/morphology (average particle size, porosity, etc.).

Although expected, no significant mechanical damage (e.g. u-cracks or delamination) is found in the anode and/or anode-electrolyte interface, according to the SEM images.

Said results are coherent with the well-known tendency of Ni agglomeration in nickel-based fuel electrodes during calendar ageing.

The AF has been quantified based on the comparison of the electrochemical parameters vs. the on-field operated samples. The correlation of the obtained results of AST protocol and the on-field samples and calculation has been done using the ASR values coming form an on-field samples operated 15 thousands hours and directly relatable with the sample aged with 8 chemical redox cycles:

$$\mathrm{AF} = \frac{t_{long\ term\ test}}{t_{AST\ bringing\ to\ the\ same\ degradation}} = 375$$

NOTE: Significant and recurrent cathode detachment at the cathode-electrolyte interface can be found for high number of cycles (> 8 cycles) which could represent a limiting factor in terms of sample electrochemical stability and therefore AST replicability. A possible cause of such detachment could be related to mechanical surface degradation of the bare side of the electrolyte during redox cycling, where the test setup is not perfectly tight. A way to overcome this problem is

to perform in-situ chemical cycling (with the full cell already mounted in the electrochemical test rig) in order to perform chemical cycles and at the same time monitor the performances, without a two-steps procedure. Results obtained with the alternative ageing procedure, mentioned in the protocol, confirm the feasibility of this approach.

2.10. *Ex-situ* interconnect 'Corrosion' aging (UNIGE)

2.10.1. Description of AST approach

The approach aims to accelerate the oxidation rate of the ferritic stainless steel used as interconnect materials by applying an overpressure to the air stream during aging in a laboratory setup. During the experiment, the ASR of the sample is monitored in AC galvanostatic mode to avoid welding of the contact mesh with the specimen and to minimize the degradation phenomena and local heating that could result from a DC current. The effect of overpressure is evaluated by comparing the ASR evolution and the rate of oxide growth on the sample surface.

2.10.2. Experimental samples

Samples can be made of the steel grade to be tested (e.g. AISI 441 or Crofer22 APU). Combined materials can also be tested as coated samples. In the frame of the project, tests have been performed on AISI 441 and Crofer22 APU coated with Cu-Mn and Co-Mn based spinels. Specimens have a round shape with a diameter of 25 mm and a maximum thickness of 5 mm.

List of tested samples is reported hereafter:

- 0002_SUN_New_002,
- 0011_SUN_New_002,
- 0013_SOL_New_002
- 0024_SOL_New_002.

2.10.3. Experimental set-up

The testing setup is designed for measuring Area Specific Resistance of samples described in section 2.10.2 and has been optimized to apply a pressure up to 5 bar to samples (Figure 30). Such instrument allows to host circular shaped samples with dimensions up to 25 mm of diameter and 5 mm thick. Samples can be heated up to 900°C and exposed to flowing and pressurized gases at both sides. The electrical contact with the sample can be achieved using gold meshes, connected to gold wires, to perform 4-wires measurements of the ASR. The setup is designed to apply the contact after the mounting and heating of the sample at any time by also regulating the mechanical load pushing the current collectors toward the sample (by using calibrated springs).

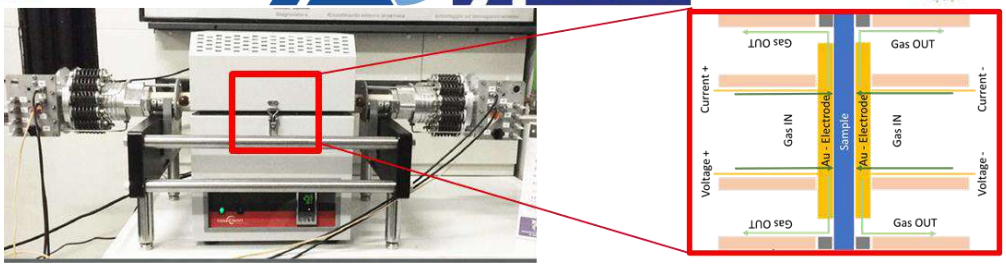

Figure 30 **Testing setup for ASR measurements exposing samples up to 900°C and 5 bar. On the right, a detailed scheme of its interior is displayed.**

2.10.4. Nominal operation parameters.

Table 29 **Nominal operation parameters**

Sample type	Operation Mode	Parameter	Units	Value	Remarks
Ferritic stainless steel disk	SOFC	Temperature	°C	850	
		Pressure	bar	1 - 4	
		Oxidant	Nml/min/cm^2	30	Air
		Current Density	µA/cm^2	500	Only applied during electrical measurements

2.10.5. Stressor (stress parameter) and stress factor

The main stress parameter of this AST is air pressure, which was found to be effective in accelerating the interconnect aging only at 850°C. The pressure range effective for accelerating the aging process is 1 to 3 bar of overpressure, above which the results are no longer consistent with respect to the degradation mechanism.

2.10.6. Presentation and quantification of the degradation at nominal conditions and under stress tests

The accelerating effect can be seen in the time evolution of ASR during the experiment. When the stressor effectively accelerates the oxidation, a faster increase in ASR is observed. A quantitative estimate of the acceleration factor can be made after the experiment by observing the aged sample in cross-section with the SEM in BSE mode. Image analysis on micrographs at 1000x or 5000x magnification provides an estimate of the oxide growth on the steel surface. By comparing the rate of oxide growth after exposure of the sample to different overpressures with a reference sample aged at ambient pressure, the acceleration factor of this test can be estimated.

2.10.7. Description of AST procedure

The procedure of AST can be summarized by the following steps:

- Placing the sample in the experimental setup, without electrical connection for the ASR measurements,

- Heating the setup to 850°C at a rate of 5°C/min,
- Waiting for temperature stabilization,
- Making electrical contact for the ASR measurements by controlled mechanical loading on both sides of the sample,
- Measuring the first ASR value to verify the initial electrical resistance,
- Applying the overpressure to the air stream,
- Starting the ASR measurement program consisting of one measurement every 25 hours for 200 or 400 hours,
- Removing the overpressure,
- Starting the cooling ramp at a rate of 5°C/min and stopping every 50°C to measure the electrical resistance as a function of temperature for the calculation of the activation energy using the Arrhenius equation.

2.10.8. Correlation of the long-term degradation at nominal operation conditions with the degradation at accelerated stress conditions

The acceleration factor resulting from the accelerated stress conditions is calculated by comparing the results obtained after different aging times and different intensities of the stressor (e.g., 200 and 400 hours; atmospheric pressure, 1 bar of overpressure). The reliability of such results can be evaluated by comparing the oxide thicknesses of ex-situ aged samples with those of specimens extracted from stacks at a known time (see annex 2.10).

2.10.9. Annex *(with illustrations)* for demonstration of the AST Protocol performance

The bar chart in Figure 31 shows the thickness of the samples of AST after aging at different overpressures for 200 hours and 400 hours. Comparing the thickness increase of the samples aged applying overpressures with those under reference conditions (atmospheric pressure), the acceleration factor can be estimated. The results can be compared with those of samples extracted from a stack to verify that the effects of aging under reference conditions are the same as those obtained by accelerating the degradation.

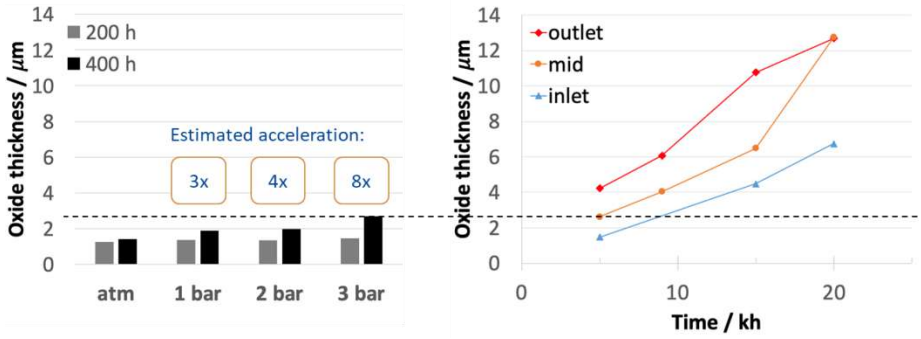

Figure 31 **Oxide thickness after aging for 200 and 400 h at different overpressure (left); oxide thickness of samples extracted from a stack in different positions (right).**

2.11. *Ex-situ* chemical redox-cycle aging (IEES)

2.11.1. Description of the AST Approach

This AST protocol concerns the accelerated aging of the fuel electrode before operation by governed redox cycling.

The main degradation mechanism for the fuel electrode during operation in both fuel cell and electrolysis mode is the reduction of the triple phase boundary points and of the Ni/gas specific surface area caused by microstructural changes in the Ni network due to Ni migration and coarsening. The migration over long distances can bring to Ni depletion near the electrolyte interface. Similar, but more severe processes of Ni coarsening and migration occur during oxidation of Ni caused by incidental change in the operation conditions (leakage, fuel starvation). Due to the expansion/shrinkage (Ni and NiO have different volume), cracks in the electrolyte/fuel electrode interface appear during the oxidation/reduction processes.

Obviously artificial redox cycling can be used as a tool for accelerated degradation of the fuel electrode, however, the process has to be strictly governed with fine tuning of the oxidation depth, so that the redox cycles would mimic the processes of normal aging.

The AST protocol for aggravated aging by artificial redox cycling of the fuel electrode is based on the introduction of precise procedure for governed mild partial oxidation.

2.11.2. Experimental samples

The developed procedure is a three-step process which uses three types of samples. The most important experiments performed on the three types of samples are included in AD ASTRA Data base.

Samples typology: the experiments for this protocol are performed on button cell size samples:

- Bare anode – half cell configuration (samples anode (0027_IEES_New_001, 0027_IEES_New_002, 0027_IEES_New_009),
- Anode/electrolyte with the barrier layer (same size) – half-cell configuration (0031_IEES_New_2, 0031_IEES_New_5, 0030_IEES_Old_1),
- Full cell (same anode/electrolyte) - (0037_IEES_New_002, 0037_IEES_Old_1, 0028_IEES_Old).

The new samples are used for determining the test conditions and development of the AST procedure. The old samples (coming from field tests) are applied for verification of the aging by comparing the field tests with the artificially aged cells and by post mortem analysis.

2.11.3. Experimental set-up

The experiments can be performed in a standard test bench for testing of SOC with option for impedance measurements. More detailed description of the used experimental set up, which is with very high precision, is given in the example in the end of the protocol (2.11.9).

The test rig should ensure measurements of bare anode in a single atmosphere (blend of hydrogen and nitrogen and air). The contacts of the bare anode and of the anode/electrolyte samples are mechanical – the samples are pressed between two Pt meshes. It is recommended the metal contact nets to be Pt, since the measurements of those two types of samples are carried out in a changeable atmosphere of N_2+H_2 and air.

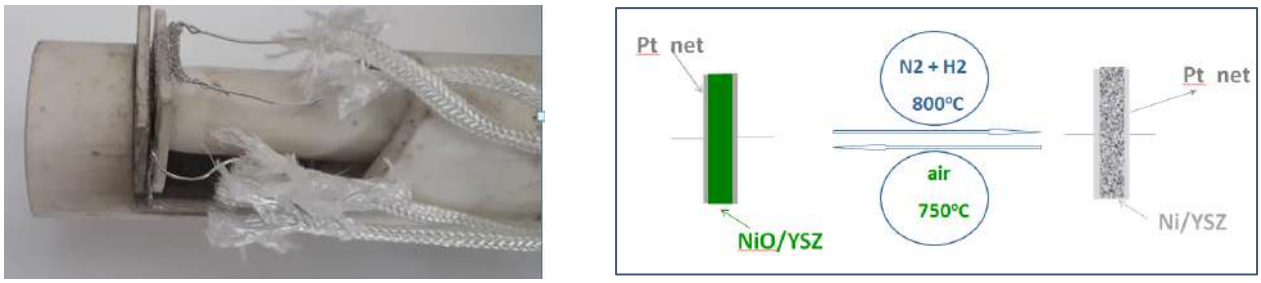

Figure 32 **Test rig head with anode sample in half cell configuration (left); schematic presentation of the redox cycling (right).**

2.11.4. Nominal operation parameters for testing of cells

Table 30 **Nominal operation parameters for testing of SoC in FC mode.**

Sample type	Operation Mode	Parameter	Units	Value	Remarks
Full Cell	FC	Temperature	°C	750	Testing of the cell before and after selected number of redox cycles: *i-V* curves and impedance in selected working points (in respect to current density)
		Pressure	Atm.	ambient	
		Oxidant (air)	Nml/min/cm^2	437,5	
		Fuel (H_2)	Nml/min/cm^2	79,4	
		Water	% in respect to the fuel	0	
		Current Density	A/cm^2	0 ; 0,2; 0,5	

2.11.5. Stressor (stress parameter) and stress factor

The stressor is the combination of consecutive steps of oxidation and reduction. The oxidation conditions are selected to ensure mild partial oxidation (Table 31).

Table 31 **Operation parameters for redox cycling.**

Sample type	Stressor	Parameter	Units	Value	Remarks
Bare anode; Anode/electrolyte, Full cell		Temperature	°C	750	
		Pressure	Atm.	ambient	
	Anode oxidation	Oxidant (air)	Nml/min/cm^2	2	Oxidation blend of: air = 2 Nml/sec/cm^2 and N_2 = 2 Nml/sec/cm^2
	Anode reduction	Fuel (H_2)	Nml/min/cm^2	2	Reduction: blend: H_2 = 2 Nml/sec/cm^2 and N_2 = 2 Nml/sec/cm^2
		Water	% in respect to the fuel	0	

The deepness of oxidation in a single cycle is adjusted by the value of the resistance in the oxidized state of bare anode sample. It should not increase more than 5 times in respect to the value in reduced state. In Figure 33 the resistance of the bare anode increases less than 2 times. The degradation depth is regulated by the number of redox cycles. There should be good reproducibility, i.e. the increase of the bare anode resistance should be the same in neighboring oxidation loops (Figure 33b). The bare anode configuration ensures precise impedance monitoring of the changes in the resistance during cycling. The determined redox cycling regime is further applied on button cell configuration for accelerated testing (see 2.11.7).

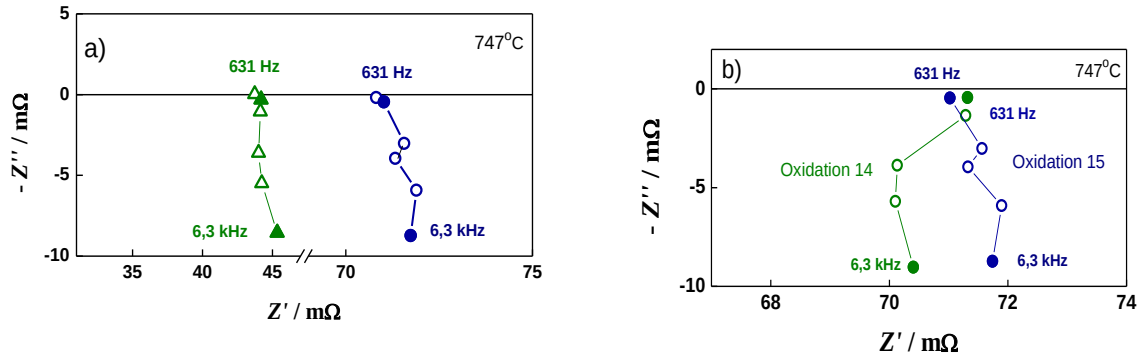

Figure 33 **Mild redox cycling following the developed protocol: a) bare anode in oxidized and reduced state; b) bare anode in two oxidized states.**

2.11.6. Presentation and quantification of the degradation at nominal conditions and under stress test

The quantification of the degradation is determined by electrochemical measurements of full cell which is subjected to anode redox cycling. The following measurements are performed:

- *I-V* curves after selected number of redox cycles (for instance in 5 cycles). Based on those measurements, the aging factor (AgF), i.e. the change of the power, of the potential and/or of the current as a function of the redox cycles number can be calculated, which gives quantitative information about the aging. For comparison with field tests and other external data the AgF is expressed in per cents.
- Impedance measurements after definite number of redox cycles (for instance 5 cycles, i.e. after the measurement of the *i-V* curve) in preliminary selected working points. Those measurements ensure information about the AgF in respect to at least the total ASR of the sample, as well as of the ohmic and the polarization ASR, which can be attributed mainly to the anode, since it is under stress conditions. More detailed impedance data analysis may distinguish the contribution of the anode and cathode in the polarization resistance, which is not, however, in the scope of the protocol.

Aging Factor (AgF)	$$\mathrm{AgF_{NC}}/\% = \frac{(ASR_{\mathrm{NC}} - ASR_{\mathrm{pristine}})}{ASR_{\mathrm{pristine}}}.100$$ NC is the number of cycles producing a given level of degradation. ASR can be replaced with: *U, j,* P_{max}. ASR can be referred to different working points of the *i-V* curve.

2.11.7. Description of the AST procedure

The procedure of governed anode aging by redox cycling is performed in 3 stets. The first two steps define and validate the experimental oxidation/reduction conditions, while the aging is performed in the third step.

- Step 1. Determination of the oxidation level by *in-situ* impedance monitoring of the changes in the Ni network resistance during oxidation of bare anode. The first and leading step in the introduction of the AST procedure is the adjustment of governed and reproducible redox cycling conditions which are determined on bare anode configuration. It gives the possibility to measure *in-situ* by impedance the Ni network resistance, i.e. the electronic conductivity of the anode, as well as its changes due to partial oxidation which increases the resistance of the sample due to partial replacement of Ni with NiO.

  The oxidation depth is selected based on preliminary chosen increase of the Ni network resistance during oxidation, which should be up to 5 times higher than the one measured after the initial reduction of the anode, i.e. before the first oxidation. The impedance measures the electronic conductivity of the NI network and thus it has inductive behavior. The oxidation should not change this state, ensuring preservation of the electronic conductivity network.

  The protocol procedure for oxidation/reduction includes 3 important moments which have to be well defined: (i) to stop the oxidation before reaching the selected increase of the resistance due to the continuation of the oxidation in nitrogen caused by the residual oxygen in the system;

(ii) to isolate the rig chamber (for about 40 seconds) after stopping the oxidation for purging the air pipeline with N_2; (iii) to introduce hydrogen shortly before the Ni network resistance reaches the selected limiting value. Hydrogen quickly reacts with the residual oxygen and prevents the sample from further oxidation. This may be accompanied with small increase (1-2^{o}C) of the temperature in the reaction zone close to the sample.

Table 32 and Table 33 give an experimental protocol used for experiment with increase of the anode resistance reaching the upper limit (5 times increase). It should be noted that the exact conditions concerning the timing of every step depend on the test rig architecture and have to be defined experimentally, following the main requirements of the protocol (maximum of the resistance increase not exceeding 5 times the initial one; preservation of the impedance inductive behavior).

Table 32 **Oxidation regime.**

Time (min/sec)	N_2 (ml/min/cm^2)	Air (ml/min/cm^2)
0	2.0	0
1’45’’	2.0	2.0
45’’	0	0
2’	2.0	0

Table 33 **Reduction regime.**

Time (min)	N_2 (ml/min/cm^2)	H_2 (ml/min/cm^2)
0’	2.0	0
6’	2.0	2.0
10’	11.2	0
5’	2.0	0

Once the appropriate experimental oxidation conditions are determined on bare anode, they serve as internal standard for redox cycling in other sample configurations where the Ni network formation and oxidation cannot be monitored anymore by impedance.

The recommended number of redox cycles is 20-50 (depending on the oxidation depth).

- Step 2. Redox cycling of anode/electrolyte sample. The main goal of this experiment is to check the effect of the selected procedure on the state of the interface anode/electrolyte which can be done by SEM after 15-20 redox cycles.
- Step 3. Redox cycling in full cell configuration. The experiments are performed on button cells. In principle they can be carried out also on big cells and stacks. The redox cycling regime follows the one chosen in Step 1.

2.11.8. Correlation of the long-term degradation at nominal operation conditions with the

The effectiveness of the fuel electrode accelerated aging in cell configuration by governed redox cycling is evaluated by the Accelerating Factor which gives the ratio between the AST timing and the calendar aging duration which brings to similar degradation. It can be evaluated by cell's electrochemical performance or by quantitative evaluation of the changes in the microstructure

(for instance, the change in the Ni particles distribution). The AST of cell under 20 redox cycles is about 50 - 60 hours. A comparison with calendar aged cells evaluates the AF to be more than 50, which is shown in the Example below.

$$\mathrm{AF} = \frac{t_{long\ term\ test}}{t_{AST\ bringing\ to\ the\ same\ degradation}} > 50$$

2.11.9. Example for application of the AST Protocol "*Ex-situ* chemical redox-cycle aging"

Selection of redox cycling regime:

Step 1. Sample configuration: "Bare anode"

Depth of oxidation: 5 times increase of the Ni network resistance during oxidation in respect to the reduced state.

Initial reduction of the green anode. The procedure starts with initial reduction of the green anode at 800°C following SOLIDPOWER recommendation. It is monitored by impedance. The diagrams in Figure 34 present the changes during reduction. The transformation of the capacitive impedance behavior in inductive (Figure 34c, 11 minutes reduction) marks the initial formation of a Ni network, which is developed in the next 20 minutes and does not change till the end of the reduction which continues 134 minutes, i.e. the resistance is constant (Figure 34d).

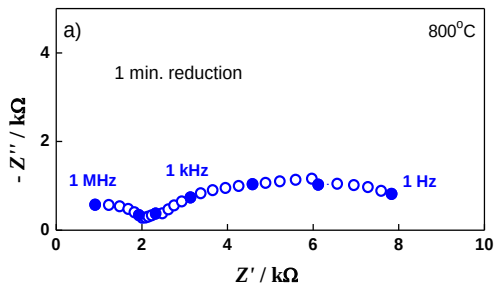

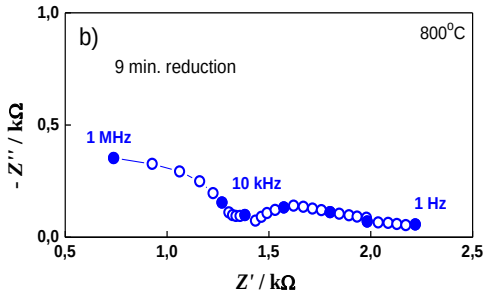

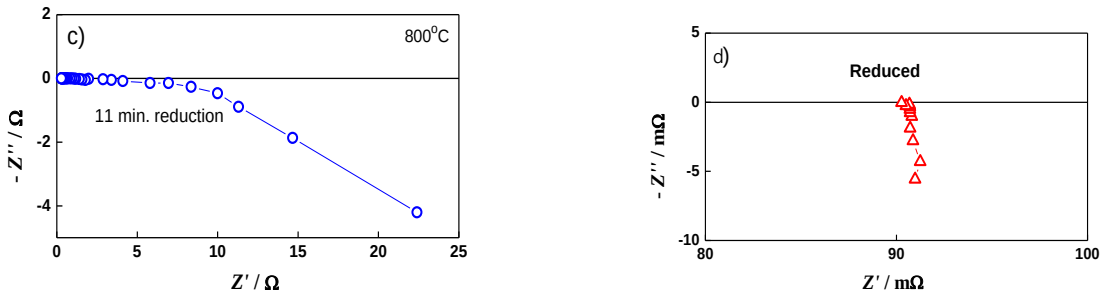

Figure 34 **Initial reduction of the bare anode.**

Definition of the redox cycling conditions.

The exact procedure needs experimental definition. The Redox cycling experiments start after the initial reduction of the anode cermet.

The recommendation is to use low oxidation and reduction flows (see Table 31 Table 32 and Table 33) and to govern the process via the duration of the oxidation. It should be marked that the oxidation continues in nitrogen. When changing the gases, it is important to blow the residual air form the pipeline. An immediate stop of the oxidation can be realized by the introduction of hydrogen in the system, i.e. by entering in regime of reduction.

The selected experimental conditions are given in Table 32 and Table 33. The reproducibility, i.e. the oxidation/reduction state in two consecutive redox cycles is presented in Figure 35a which demonstrated the good reproducibility.

Registration of aging:

- By post mortem analysis of the microstructure. SEM/EDX can visualize the Ni particles agglomeration (Figure 36), as well as the change in the size distribution.
- By increase of the Ni network resistance (Figure 35b). For bare anode this approach is not enough sensitive for small deepness of oxidation.

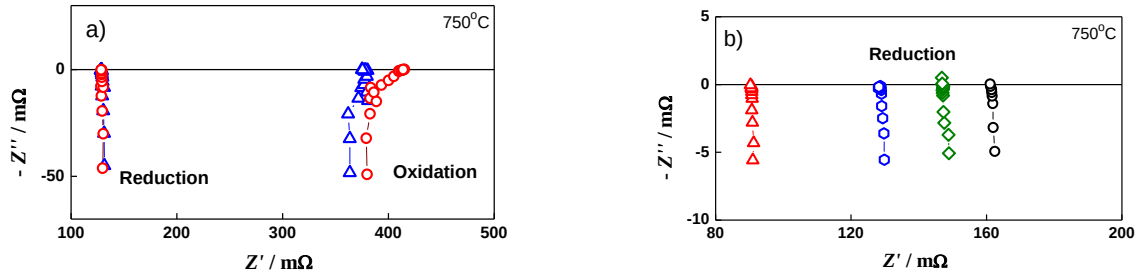

Figure 35 **Impedance diagrams of bare anode during redox cycling: a) two consecutive redox cycles - Cycle 7 (▲) and Cycle 8 (•); b) reduced state after four different redox cycles - Cycle 2 (▲), Cycle 7 (▲), Cycle 11 (▲), Cycle 18 (▲).**

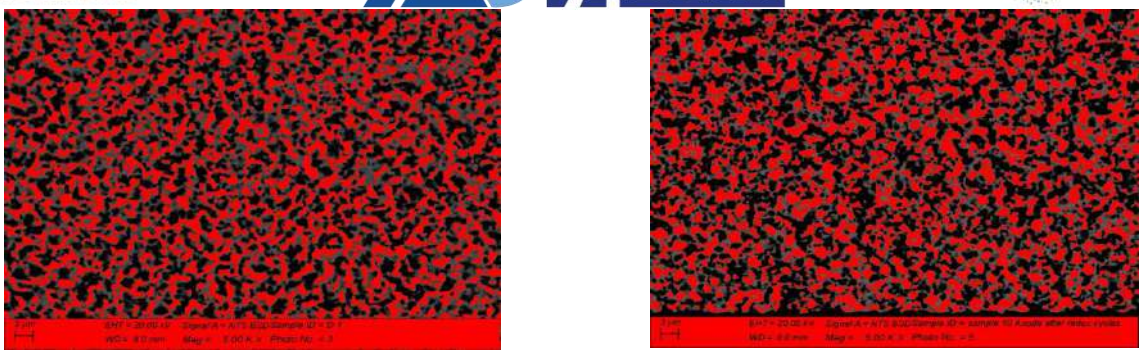

Figure 36 **SEM-BSE images of bare anode: reduced (left side) and after 10 redox cycles (right side): red - Ni; black - pores; grey - YSZ.**

Step 2. Experiments on Anode/electrolyte sample

In this configuration the Ni network is not any more visible by impedance and its changes during oxidation/reduction cannot be seen. However, the conditions are defined in Step 1 and their reproducibility is confirmed.

The redox cycling is performed to check the effect of the selected procedure on the state of the interface anode/electrolyte. The number of cycles should be similar to the one planned in Step 3 on fuel cell configuration. The validation is performed by SEM after 20 redox cycles (Figure 37).

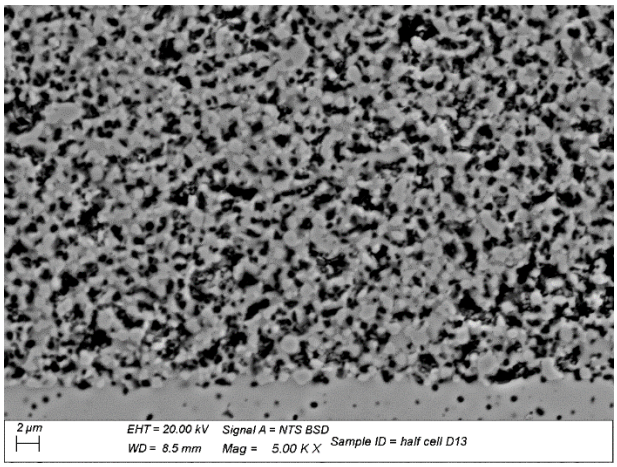

Figure 37 **SEM image of the interface anode/electrolyte after 20 redox cycles.**

Step 3. Redox cycling in Full cell configuration

The experiment is performed on button cell. The procedure applies accelerated aging of the fuel electrode in full cell configuration by governed redox cycling which is performed on pristine sample after the initial reduction of the green anode, i.e. before operation. The investigation is based on 20 redox cycles.


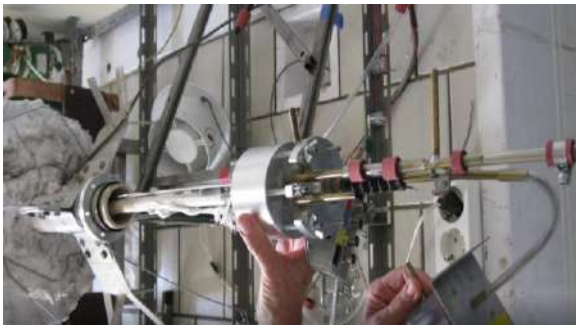

Figure 38 **Test bench: general view (left); mounting of the test rig in the furnace (right).**

Monitoring, controlling and evaluation of the redox cycling: two approaches are applied: electrochemical and microstructural. A comparative electrochemical and microstructural analysis of: (i) pristine and redox cycled cell and (ii) redox cycled with calendar aged cells is performed.

Electrochemical testing: The experiments are performed in a set up (Figure 38) with especially designed furnace with DC power supply, provided with a power galvanostatic operating at 100 A and 15 V. Thus, the noises due to the power net supply (50 Hz and the harmonics) are completely eliminated. The measurement of the furnace temperature is done with a Pt-Pt/Ro thermocouple, located in the space between the two alumina tubes - external, supporting the furnace heater and internal, containing the sample rig. For temperature control a PID thermostat is used, with a sensitivity of 1°C. For precise measurement of the sample temperature, a second thermo - couple (K-type) is positioned inside the rig, in close vicinity to the sample. The resolution of the primary ADC convertor which is connected to the computer is ~ 0,14°C. By applying an algorithm for a triple measurement and reading of the mean value, an extreme effective resolution of 0,01°C is obtained. The computer is equipped by a special home-made temperature monitoring software. The system performs temperature measurements every minute and ensures their plotting and monitoring in coordinates temperature/time, as well as plotting and monitoring of the temperature derivative (in °C per minute). The system supports the selection of the exact moment for starting the impedance measurement – when the desired temperature is reached, and the temperature gradient does not exceed 0,6 °C. The impedance measurements are performed on IVIUM frequency response analyser in frequencies from 1 MHz down to 0,1 Hz.

The button cell testing setup consists of a completely ceramic housing (Figure 38b). The cell is sealed on the oxygen electrode side by ceramic paste (Ceramabond) following the procedure of the producer (Aremco products Inc). The testing conditions for redox cycling and evaluation of the degree of degradation are given in Table 30 and Table 31. The validation of the degradation level is performed in FC mode. However, the procedure can be done for electrolysis mode.

The degree of aging by anode redox cycling in respect to the initial state of the sample is extracted from the periodically measured *i-V* curves (Figure 39 left) via calculations of the potential *U* change at constant current *I* as a function of the number of cycles. It is convenient to present the results in % (Table 34).

Table 34 **Voltage decrease at constant current density extracted from the *i-V* curves.**

	Initial	7 redox		20 redox	
i, A/cm^2	*U*, mV	*U*, mV	Change vs. initial, %	*U*, mV	Change vs. initial, %
0,28	961	956	0,52	937	2,5
0,50	864	848	1,85	830	4,5

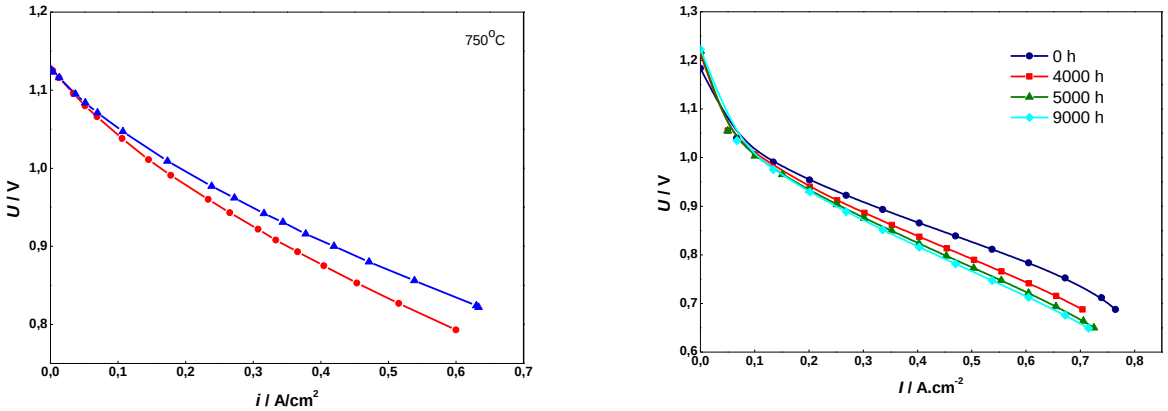

Figure 39 **Current-voltage (*i-V*) curves of: artificially aged cell before redox cycling (▲) and after 20 redox cycles (•) (left); calendar aged cell operated for 9000 h (right).**

Similar comparison with the *i-V* curves for calendar aged cells for 9000 hours (Figure 39 right) is also done (Table 35). The data show similarity in respect to deepness of degradation between the artificial aging with 20 redox cycles and calendar aging of 4000 hours.

Table 35 **Voltage decrease at constant current density extracted from *i-V* curves measured during 9000 hours field testing.**

	Initial	4000 h		6000 h		9000 h	
i, A/cm^2	*U*, mV	*U*, mV	*Change vs. initial*, %	*U*, mV	*Change vs. initial*, %	*U*, mV	*Change vs. initial*, %
0,28	917	898	2,07	883	3,70	882	3,82
0,50	827	791	4,35	768	7,13	766	7,38

Impedance measurements in selected working points (Table 30) distinguish the contributions from different parts of the cell and the changes in their ASR caused by redox cycling (Table 36).

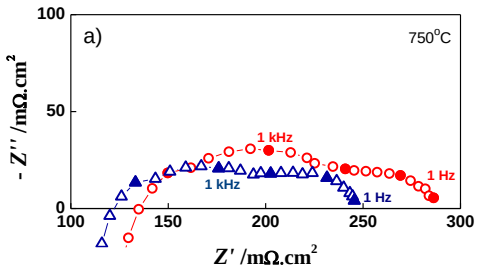

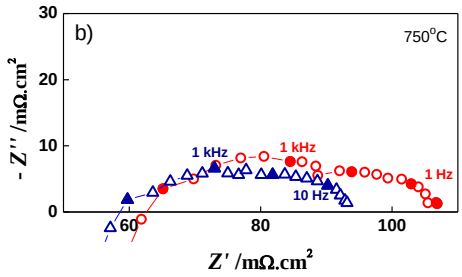

Figure 40 **Impedance diagrams of button cell before Redox cycling (▲), after 7 Redox cycles (■) and after 20 Redox cycles (●) under load of: a) 0,28 A/cm²; b) 0,50 A/cm².**

Table 36 **ASR (ohmic R_Ω, polarization R_p and total R_T) of button cell after the initial reduction, after the 7th and 20th redox cycle.**

	R (mΩ.cm²)			% Change (vs. 0 cycles)	
	0 Redox cycles	**7 Redox cycles**	**20 Redox cycles**	**7 Redox cycles**	**20 Redox cycles**
R_Ω	58,7	59,8	63,5	+ 1,9	+ 8,2
R_p	59,8	39,7	42,5	+ 16,4	+ 24,5
R_T	92,8	99,5	106,0	+ 7,2	+ 14,2

Microstructural characterization

The post mortem microstructure and porosity analyses are performed on scanning electron microscope (SEM) Zeiss EVO 40 with acceleration voltage of 20 kV, equipped with an energy dispersive X-ray spectroscope (EDXS Pentafet).

The comparative analysis of calendar aged and redox cycling aged cell confirms the aging. More than 85 % of the Ni grains in the pristine cell A measured by calibrated image analysis have a maximum surface below 1 µm² (Figure 41 Cell A). In the redox cycled, as well as in the calendar aged cells this number decreases while the quantity of the larger grains increases with up to 10 % (Figure 41, Cells B, C, E). The comparative analysis of the histograms with Ni grains distribution shows that for the sample after 20 redox cycles grains with size about 20 µm are observed (Figure 42b). Since the Ni grains have irregular shape, their size is presented as surface area (µm²). Bigger grains are formed also in sample D and sample E which is tested in electrolysis mode. Cracks at the anode/electrolyte are observed in samples D and E, while the artificially aged sample B has unaffected interface.

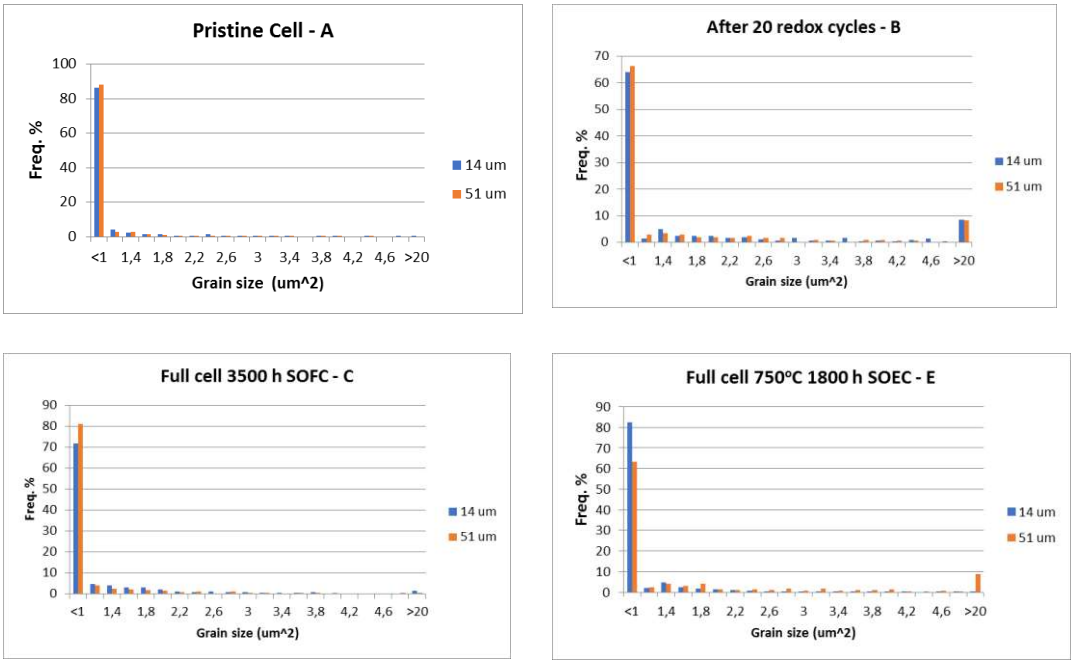

Figure 41 **Ni grain size surface distribution (µm^2) at 14 µm (■) and 51 µm (■) from the anode/electrolyte interface.**

The obtained results confirm that an *ex-situ* artificial aging of SOC by redox cycling can be applied for accelerated stress tests.

The main advantage of the developed procedure is that it can be governed and fine-tuned, giving highly reproducible cycles. The performed AST procedure shows correlation of the 20 redox cycles with the selected depth of oxidation with cell performance degradation corresponding to about 3500 - 4000 hours calendar aging. Taking into consideration that the duration of 20 redox cycles is about 60 working hours, the AF could be estimated to be more than 50.

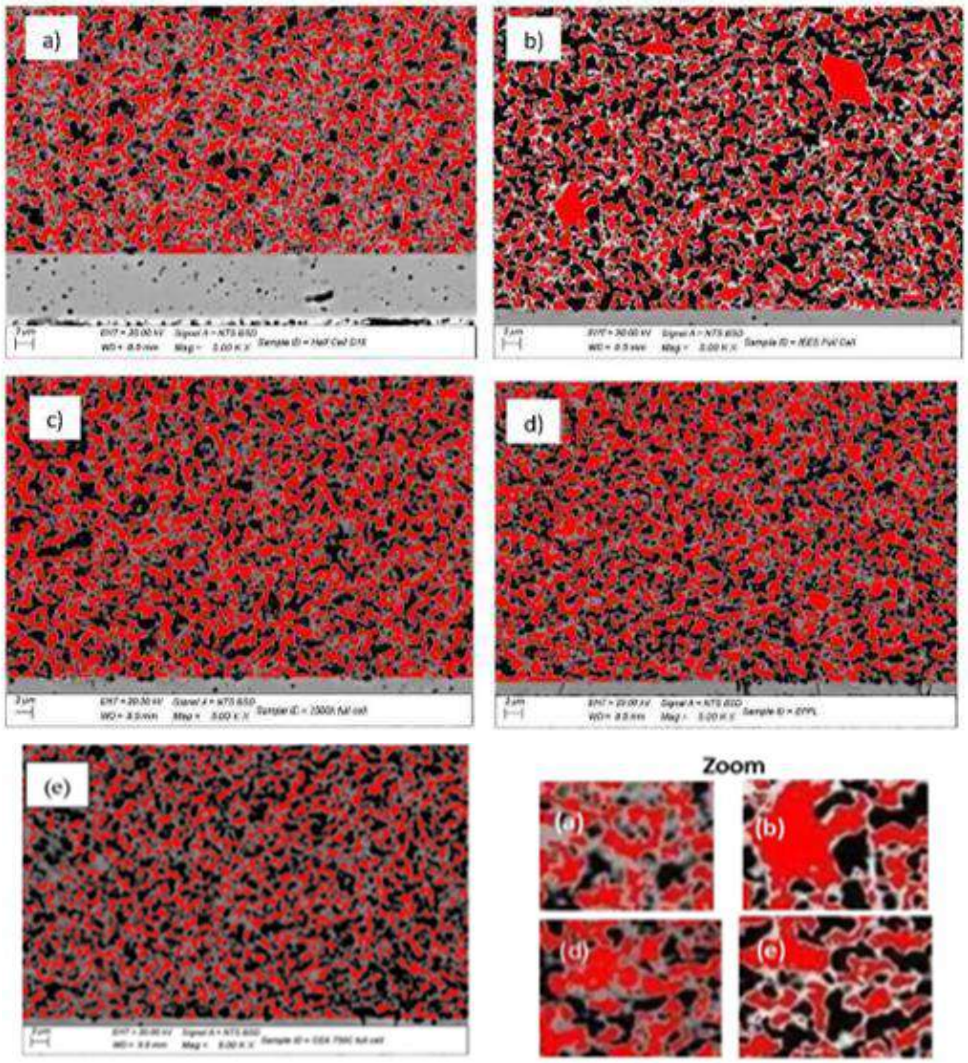

Figure 42 **SEM-BSE images of: a) sample A (pristine); b) sample B (20 redox cycles); c) sample C (3500 h); d) sample D (3000 h); e) sample E (1800 h in electrolyser mode).**

2.12. *Ex-situ* cell 'high steam & temperature' fuel electrode aging (DTU)

2.12.1. Description of the AST Approach

The impact of high steam at the fuel electrode and temperature were used as potential stressors for degradation of the fuel electrode in case of two configurations. ASC and ESC under nominal load conditions. The acceleration studies were performed under OCV conditions which means that no load was applied on the cell under durability operation of 1000 h. It is expected to accelerate the Ni coarsening and migration effects as compared to low steam conditions and to compare to cell aged with load to have faster as well as cheaper cell degradation (such that it can be performed in reducing furnaces without test rigs).

2.12.2. Experimental samples

The samples aged under the in-situ aging conditions were single cells with an active area of 4x4 cm^2 received from SolidPower (ASC) and Sunfire (ESC). Initially the cell aging was also performed in furnaces, however due to the need to also perform electrochemical characterization, the cells were in the next iteration.

ESC samples

In tube furnace:

0004_SUN_NEW_003,

0004_SUN_NEW_004,

0004_SUN_NEW_001,

0004_SUN_NEW_002,

0004_SUN_NEW_005.

In rigs:

0035_SUN_New_002,

0035_SUN_New_003.

ASC samples

In rigs:

0033_SOL_NEW_001,

0033_SOL_New_006.

2.12.3. Experimental set-up

In the first iteration, ex-situ tests were carried out on half cells (fuel electrode + electrolyte + barrier layer) from both suppliers. All ex-situ tests were carried out in tube furnaces as shown in Figure 43 under a single atmosphere. Figure 44 shows the setup used for the *ex-situ* aging using single cell test setups similar to the *in-situ* aging tests.

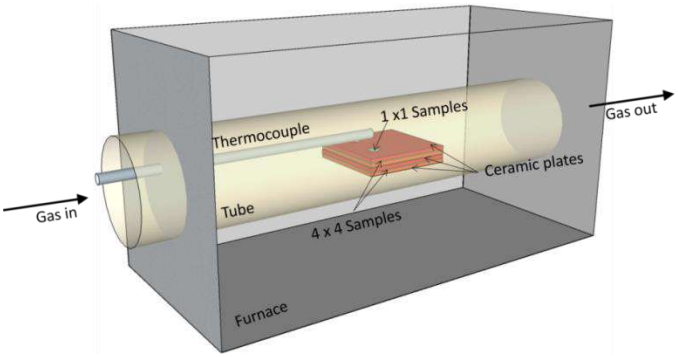

***Figure 43 Ex-situ* aging in single atmosphere setup (half cells).**

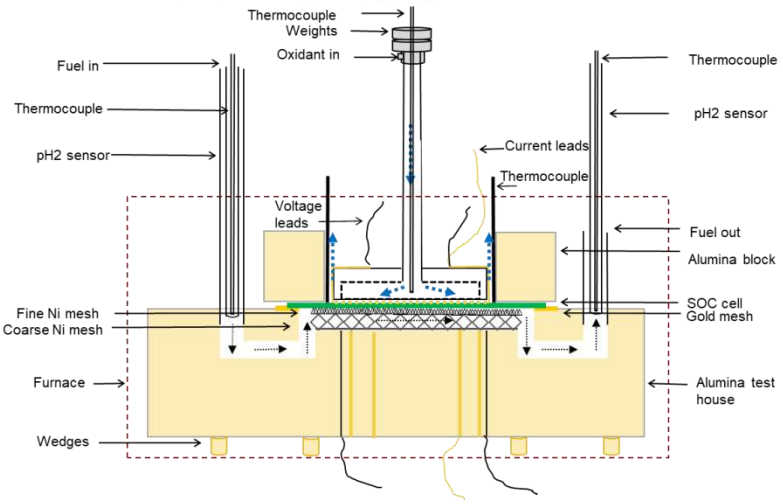

Figure 44 **Ex-situ aging in dual atmosphere setup (full cells).**

2.12.4. Nominal operation parameters

The nominal operation is taken from the *in-situ* aging conditions as in section 2.5 performed with load under low steam composition. This is summarized in Table 37 and Table 38 for ASC and ESC configurations, respectively.

Table 37 **Nominal operation parameters for ASC configuration.**

Sample type	Operation Mode	Parameter	Units	Value	Remarks
ASC Full cell		Temperature	°C	750	4x4 cm^2 active area
		Pressure		1	
		Fuel	Nml/min/cm^2	0,02 H_2 0,0008 H_2O	Single gas or gas mixture
		Water	% in respect to the fuel	4	
		Oxidant	Nml/min/cm^2	0,06 AIR	Single gas or gas mixture
		Current Density	A/cm^2	N/A	
		Fuel Utilization	%	14	
		Oxidant Utilization	%		
		Other depending on the protocol	%	4	Partial pressure of steam

Table 38 **Nominal operation parameters for ESC configuration.**

Sample type	Operation Mode	Parameter	Units	Value	Remarks
ESC Full cell		Temperature	°C	850	4 x 4 cm^2 active area
		Pressure		1	
		Fuel	Nml/min/cm^2	0,01 H2 0,0004 H2O	Single gas or gas mixture
		Water	% in respect to the fuel	4	
		Oxidant	Nml/min/cm^2	0,06 AIR	Single gas or gas mixture
		Current Density	A/cm^2	0,2	
		Fuel Utilization	%	14	
		Oxidant Utilization	%		
		Other depending on the protocol	%	2,7	Partial pressure of steam

2.12.5. Stressor (stress parameter) and stress factor

The stressor used in this study was the steam content the fuel electrode and temperature (in case of ESC) under OCV on both the ASC as well as the ESC configurations. The chosen parameters are summarised in the Table 39

Table 39 **Stressor-steam composition and temperature used in case of single cell tests on the two cell configurations.**

Parameters	Ex-situ treatment		
	ASC	ESC	
H_2O/H_2	10:90	60:40	60:40
H_2 flow [l/h]	12	6	6
H_2O flow [l/h]	8	4	4
N_2 flow [l/h]	0	3	3
Total flow rate [l/h]	20	13	13
pH_2O	90	30	30
Current density [A/cm^2]	0	0	0
Temperature [°C]	750	850	950

Further, the half cells that were aged in the tube furnaces were aged as per the conditions specified in Table 40. These results were not discussed further due to the challenge of deposition of air electrodes on the half cells post aging for electrochemical characterization.

Table 40 **Summary of the operating conditions for the *ex situ* aging in the tube furnaces.**

ESC half cell (Ex-situ testing matrix)					
		1	2	3	Nominal (in rig as ref)
Temperature (°C)		850	950	0	
Current density (A/cm²)		0	0	0	0
Fuel composition (mol %)	H_2O	40	75	90	$80H_2/20H_2O$, $50H_2/50H_2O$, $96H_2/4H_2O$
Time (hrs)		24-50	500-1000	2000	0

2.12.6. Presentation and quantification of the degradation at nominal conditions and under stress test

Degradation rate[1]	$\mathrm{DR}/\%/kh = \frac{(\mathrm{ASR}_{aged} - \mathrm{ASR}_{\mathrm{ref}})}{\mathrm{ASR}_{\mathrm{ref}}} 100 \cdot \frac{1000}{t_{aging}}$ $\mathrm{DR}/m\Omega cm2/kh = (\mathrm{ASR}_{aged} - \mathrm{ASR}_{\mathrm{ref}}) . \frac{1000}{t_{aging}}$ [1]ASR is also computed separately as ohmic and polarisation resistances obtained from the EIS measurements.

For the quantification of the degradation, the cell resistances were computed from *i-V* curves as well as EIS measurements. However, the EIS measurements were chosen for a more detailed comparison to understand the changes observed in the different degradation contributions. In addition, the SEM post mortem analysis was also performed to compare the changes in the Ni sizes and fractions.

2.12.7. Description of the AST procedure

The sample was tested as per the protocol conditions defined within the consortium in the following steps:

- Heat up under N_2 on the fuel electrode and Air at the air electrode up to desired temperature of 750°C (ASC) and 850°C (ESC),
- Shift to safety H_2 for two hours and then to pure H_2 for 1 hour to ensure complete reduction of the fuel electrode,
- Perform characterisation of the cell using EIS spectra at specified fingerprint conditions, i.e 96/4 H_2/H_2O, 80/20 H_2/H_2O, 50/50 H_2/H_2O with air and O_2 at different temperatures. *I-V* curves were not performed to avoid effect of current on the cells,
- Set specified fuel compositions and perform EIS at intervals for 1000 h durability operation,
- Cool down as per protocol using safety H_2 and air at air electrode,
- Perform post mortem analysis with SEM.

Table 41 summarises the protocol for the different parameters used in the *ex-situ* aging tests for the fuel electrode with different hydrogen/steam ratios to study the effect of steam.

Table 41 **Protocol for ASC and ESC – *ex-situ* cell 'steam' fuel electrode aging (DTU).**

	Test input parameters		Comments
steam- approach	temperature	750°C (ASC basis) 850°C (ESC basis) 950°C (ESC basis)	
	pressure	ambient	
	fuel	10/90 H_2/H_2O **ASC basis** 60/40 H_2/H_2O **ESC basis**	The flow rates are specified in a separate table under stressors section
	oxidant	$f_{air,pos,in}$ x = 178,5 mmol/h/cm^2	
	current density	OCV	

2.12.8. Correlation of the long-term degradation at nominal operation conditions with the degradation at accelerated stress conditions

Anode supported cell

The contribution from the fuel electrode TPB at high frequencies is lower with the increase in steam composition and significantly low for the 10/90 H_2/H_2O aged at OCV conditions (see Figure 45) highlighting the favorable reaction kinetics under high steam conditions.

The fuel conversion and diffusion contributions were identified at ~ 1 Hz with significantly higher steam at the inlet of 90 %.

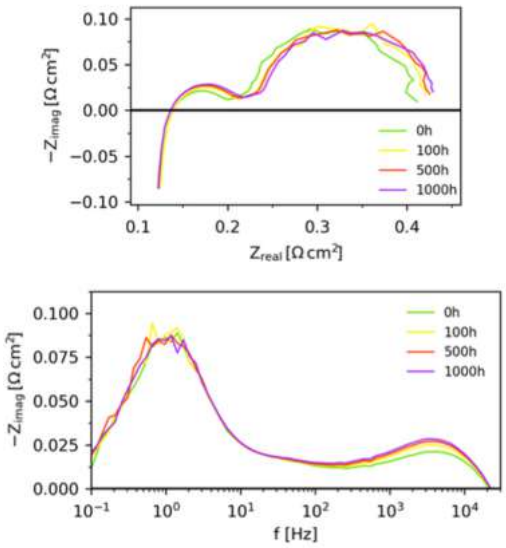

Figure 45 **Nyquist (top) and Bode plots (below) spectra recorded under long term aging at 0 h, 100 h, 500 h and 1000h for 10/90 H_2/H_2O under OCV (*ex-situ*) conditions.**

The *ex-situ* aged cell under OCV showed a 88 % (0,046 Ω.cm^2) increase at the high steam content of 90 %. A charge transfer resistance increase of ~ 71 % (0,038 Ω.cm^2) was observed for the FC operated cell with 40 % steam. This further confirms that the presence of high steam accounts for the primary mechanism of the degradation leading to the increase in the charge transfer contribution in ASC configuration with Ni-YSZ fuel electrodes. Figure 46 compares the *ex-situ* aged cells with the *in-situ* aged ASCs explained in section 2.5.

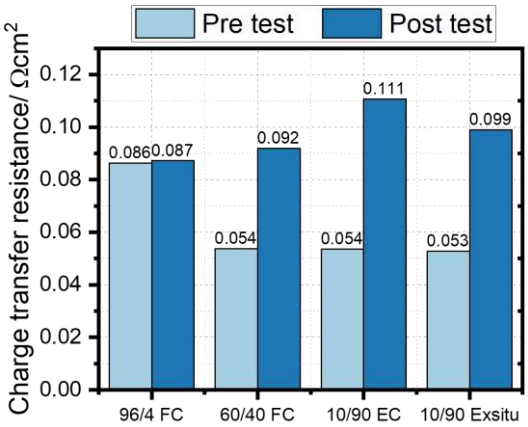

Figure 46 **Charge transfer resistances deconvoluted using suitable ECM from pre and post durability EIS recorded at 80/20 H_2/H_2O and air at 750°C.**

Electrolyte supported cell

During the *ex-situ* treatment at two temperatures (850°C and 950°C), only three EIS were recorded (at the start, 500 h and at the end of the durability testing over 1000 h). Ohmic contributions obtained from EIS of the cells during both the *ex-situ* treatments showed a significant increase at a rate of ca. 92 mΩcm^2/kh for first 500 h in both *ex-situ* aged cells (25 %kh^{-1} and 45 %kh^{-1} for 850°C and 950°C, respectively) Figure 47a and b. The degradation rate of ohmic resistance during the

treatment at 950°C starts to decrease with time, to 72 mΩcm^2/kh at 1000 h (35 %.kh^{-1}). Thus, a detailed microstructural analysis is required along with spectroscopy techniques to analyse further the influence of these conditions under OCV conditions.

For the case of *ex-situ* treated cells (Figure 47 a and b), a rate of ca. 35-37 mΩcm^2/kh (~ 45 %.kh^{-1}) was observed in the first 500 h for the polarisation resistances. In the next 500 h, the slope of the *ex-situ* operated cells reduced slightly. The absolute change in the polarization contributions of both *in-situ* and *ex-situ* aged cells with 40 % steam was 0,036-0,038 Ω.cm^2, which indicates that an increase in Rp aging was achieved by treating the cells under higher steam partial pressures (0,3 atm) with or without polarization as compared to the dry steam conditions. Furthermore, for a direct comparison, the fingerprint tests recorded at OCV pre- and post- durability tests were analysed.

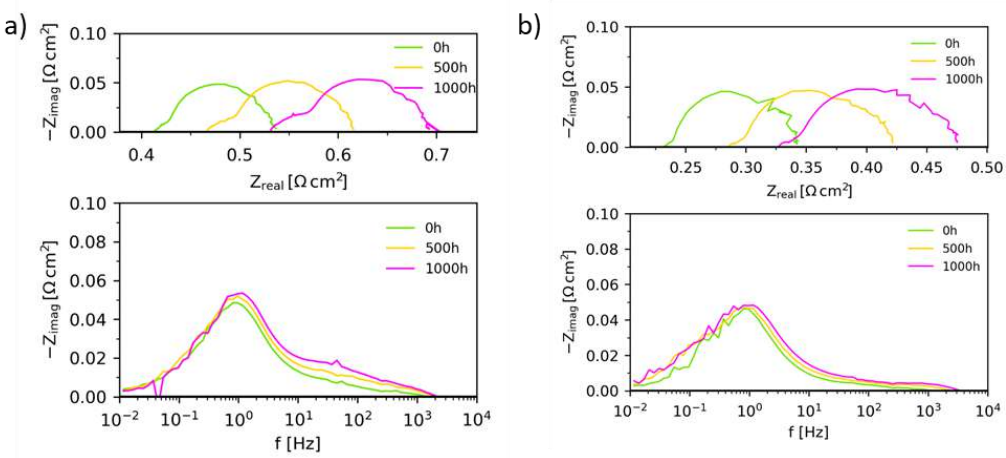

Figure 47 **Nyquist (top) and Bode plots (below) spectra recorded under long term ex situ aging (OCV conditions) at 0 h, 500 h and 1000 h for a) 60/40 H_2/H_2O at 850°C and b) 60/40 H_2/H_2O at 950°C.**

The effect of higher temperature (950°C) was studied using the *ex-situ* aging approach (Figure 48). Higher aging temperature is seen to induce severe changes in the diffusion and electrochemical contributions (~ 0,1 Hz) in comparison to the *in-situ* operated cells as well as the *ex-situ* aged cells under similar fuel compositions. Variation at the air electrode and ionic rail ~ 100 Hz and 1 kHz was observed as well. In addition to the increase in ohmic contributions, the polarisation resistance of the cell increased by ~ 96 mΩcm^2/kh. This is ~ 3 times higher than the other *in-situ* and *ex-situ* long term aged cells under the same inlet fuel composition of 60/40 H_2/H_2O. Thus, loss of the reaction sites at the fuel electrode were accelerated significantly by high temperature and in combination with certain content of steam in the hydrogen fuel. For more detailed understanding of the changes, microstructural changes for the cells aged using the two approaches are to be examined.

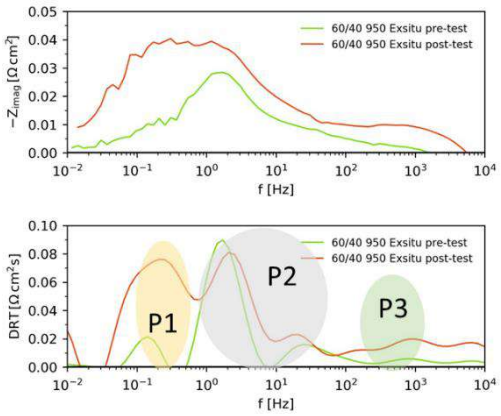

Figure 48 **Bode and DRT plots (top and bottom) for EIS recorded pre and post durability testing at 850°C with 80/20 H_2/H_2O at OCV for cell operated at 60/40 H_2/H_2O composition at 950°C under *ex-situ* aging for 1000 h.**

LIST OF ABBREVIATIONS

Abbreviation	Meaning
AC	Alternating Current
ACS	Anode Supported Cell
AF	Acceleration Factor
AgF	Aging Factor
ASR	Area Specific Resistance
AST	Accelerated Stress Tests
CGO	$Ce_{0.8}Gd_{0.2}O_{2-\delta}$
DC	Direct Current
DoE	Design of Experiments
DRT	Distribution of Relaxation Times
EC	Electrolyser Cell
EIS	Electrochemical Impedance Spectroscopy
ESC	Electrolyte Supported Cell
FC	Fuel Cell
FU	Fuel Utilization
GDC	$Gd_{0.2}Ce_{0.8}O_{2-\delta}$
LSC	$La_{0.5}Sr_{0.5}CoO_3$
LSCF	$La_{0.6}Sr_{0.4}Co_{0.2}Fe_{0.8}O_{3-\delta}$
LSM	$(La_{0.80}Sr_{0.20})_{0.98}MnO_{3-\delta}$
MFC	Mass Flow Controller
OCV	Open Circuit Voltage
OU	Oxidant Utilization
SC	Steam Conversion
SEM	Scanning Electron Microscope
SEM-EDX	Scanning Electron Microscopy with Energy Dispersive X-Ray Analysis
SOE	Solid Oxide Electrolyser
SOEC	Solid Oxide Electrolyser Cell
SOC	Solid Oxide Cell
SOFC	Solid Oxide Fuel Cell
TEC	Thermal Expansion Coefficient
THD	Total Harmonic Distortion
TPB	Triple Phase Boundary
YSZ	Yttria Stabilized Zirconia